



# Ocular mucoadhesive and biodegradable spanlastics loaded cationic spongy insert for enhancing and sustaining the anti-inflammatory effect of prednisolone Na phosphate; Preparation, I-optimal optimization, and In-vivo evaluation

Mayada Said<sup>a</sup>, Khaled M. Ali<sup>b</sup>, Munerah M. Alfadhel<sup>c</sup>, Obaid Afzal<sup>d</sup>, Basmah Nasser Aldosari<sup>e</sup>, Maha Alsunbul<sup>f</sup>, Rawan Bafail<sup>g</sup>, Randa Mohammed Zaki<sup>c,h,\*</sup>

<sup>a</sup> Department of Pharmaceutics and Industrial Pharmacy, Faculty of Pharmacy, Cairo University, P.O. Box 11562, Cairo, Egypt

<sup>b</sup> Department of Surgery, Anesthesiology and Radiology, Faculty of Veterinary medicine, Cairo University, PO Box 12211, Giza, Egypt

<sup>c</sup> Department of Pharmaceutics, College of Pharmacy, Prince Sattam Bin Abdulaziz University, P.O. Box 173, Al-Kharj 11942, Saudi Arabia

<sup>d</sup> Department of Pharmaceutical Chemistry, College of Pharmacy, Prince Sattam Bin Abdulaziz University, Al Kharj 11942, Saudi Arabia

<sup>e</sup> Department of Pharmaceutics, College of Pharmacy, King Saud University, P.O. Box 2457, Riyadh 11451, Saudi Arabia

<sup>f</sup> Department of Pharmaceutical Sciences, College of Pharmacy, Princess Nourah bint Abdulrahman University, P.O. Box 84428, Riyadh 11671, Saudi Arabia

<sup>g</sup> Department of Pharmaceutics and Pharmaceutical Industries, College of Pharmacy, Taibah University, P.O. Box 30039, Al-Madinah, Al-munawarah 41477, Saudi Arabia

<sup>h</sup> Department of Pharmaceutics and Industrial Pharmacy, Faculty of Pharmacy, Beni-Suef University, Beni-Suef 62514, Egypt

## ARTICLE INFO

### Keywords:

Ocular  
I-optimal design  
Prednisolone  
Anti-inflammatory  
Spanlastics  
Spongy insert  
Mucoadhesive  
Biodegradable  
Nanotechnology  
Histopathology  
Immunohistochemistry

## ABSTRACT

This study aimed to formulate and statistically optimize spanlastics loaded spongy insert (SPLs-SI) of prednisolone Na phosphate (PRED) to enhance and sustain its anti-inflammatory effect in a controlled manner. An I-optimal optimization was employed using Design-Expert® software. The formulation variables were sonication time, the Span 60: EA ratio and type of edge activator (Tween 80 or PVA) while Entrapment efficiency (EE%), Vesicles' size (VS) and Zeta potential (ZP) were set as the dependent responses. This resulted in an optimum spanlastics (SPLs) formulation with a desirability of 0.919. It had a Span60:Tween80 ratio of 6:1 with a sonication time of 9.5 min. It was evaluated in terms of its EE%, VS, ZP, release behavior in comparison to drug solution in addition to the effect of aging on its characteristics. It had EE% of 87.56, VS of 152.2 nm and ZP of -37.38 Mv. It showed sustained release behavior of PRED in comparison to drug solution with good stability for thirty days. TEM images of the optimized PRED SPLs formulation showed spherical non-aggregated nanovesicles. Then it was loaded into chitosan spongy insert and evaluated in terms of its visual appearance, pH and mucoadhesion properties. It showed good mucoadhesive properties and pH in the safe ocular region. The FTIR, DSC and XRD spectra showed that PRED was successfully entrapped inside the SPLs vesicles. It was then exposed to an in-vivo studies where it was capable of enhancing the anti-inflammatory effect of PRED in a sustained manner with once daily application compared to commercial PRED solution. The spongy insert has the potential to be a promising carrier for the ocular delivery of PRED.

## 1. Introduction

Eye inflammation is a prevalent condition that affects people of all ages and genders. Periorbital discomfort, proptosis, eyelid ptosis or edema, and impaired ocular mobility are all features of this condition (Hanafy et al. Chaudhari and Desai, 2019). Topical corticosteroids are

the most often used treatment for ocular inflammation. Treatment with standard topical prednisolone and dexamethasone is typically initiated with hourly administration of drops for the first four days to reduce the intense inflammation, followed by gradual reduction in medication and discontinuation of therapy (Hanafy et al. Chaudhari and Desai, 2019).

Uveitis is a term used to define a set of inflammatory eye diseases.

\* Corresponding author at: Department of Pharmaceutics College of Pharmacy, Prince Sattam Bin Abdulaziz University, P.O. Box 173, Al-Kharj 11942, Saudi Arabia.

E-mail addresses: [mayada.mohamed@pharma.cu.edu.eg](mailto:mayada.mohamed@pharma.cu.edu.eg) (M. Said), [r.abdelrahman@psau.edu.sa](mailto:r.abdelrahman@psau.edu.sa) (R.M. Zaki).

<https://doi.org/10.1016/j.ijpx.2024.100293>

Received 7 August 2024; Received in revised form 10 October 2024; Accepted 15 October 2024

Available online 16 October 2024

2590-1567/© 2024 The Authors. Published by Elsevier B.V. This is an open access article under the CC BY-NC-ND license (<http://creativecommons.org/licenses/by-nc-nd/4.0/>).

Furthermore, Uveitis is classified into four types based on the anatomical areas of the eye that might turn out to be inflamed. Pan uveitis, posterior uveitis, intermediate uveitis, and anterior uveitis are examples of these. The ciliary body, iris, and anterior vitreous are all affected by anterior uveitis (Teabagy et al., 2023). The vitreous is the predominant site of inflammation in intermediate uveitis, whereas the retina or choroids are affected in posterior uveitis (Jabs et al., 2005). Uveitis can be classified as infectious or non-infectious. Intermediate and posterior uveitis might be a primary ocular condition or a symptom of a systemic disease. Because of the high occurrence of problems such as cystoid macular edema (CME), retinal detachment, subretinal and epiretinal fibrosis, glaucoma, optic atrophy, and cataracts, they represent majority of the visual loss related to uveitis. According to a European study for more than 500 patients suffered with posterior uveitis, up to 35 % had visual loss or visual impairment (Rothova et al., 1996). Furthermore, uveitis is responsible for 10–15 % of blindness in the United States (Suttrop-Schulten and Rothova, 1996).

The primary goal of uveitis treatment is to reduce intraocular inflammation, relieve discomfort, and inhibit visually substantial consequences. When anti-inflammatory drugs are required to be administered systemically, they frequently require large doses over long periods of time to provide an appropriate anti-inflammatory impact. Corticosteroids are the mainstay of uveitis treatment; nevertheless, medication may be ineffective or have treatment-limiting adverse effects. Chronic systemic corticosteroid therapy has been related to many of adverse effects, including changes in general appearance, weight gain, systemic hypertension, hyperglycemia, gastritis, opportunistic infections, and psychosis. Treatment for uveitis can be administered topically, periocularly, intraocularly, or systemically. There are complications that are common to all routes of delivery as well as ones that are unique to each one (Conrady and Yeh, 2021).

The human eye is a sensitive and sophisticated organ. The existence of numerous structural and physiological barriers around the eye, such as narrow spaces between the corneal epithelial cells, blinking, tear secretion, and tear film formation, decreases drug residence time and thus conveyance to the targeted site, making drug delivery to the eye very limited (Gaudana et al., 2010; Le Boursais et al., 1998; Liu et al., 2012; Seyfoddin et al., 2010). The cornea's dual nature, due to its superficial layers of lipophilic epithelium and hydrophilic stroma, inhibits the penetration of many drug substances (Said et al., 2021).

Topical eye drops instillation is the most common route for ocular drug application which could be referred because of ease of installation, non-invasiveness, and thus patient compliance. However, there are significant disadvantages of using eye drops, such as rapid drug drainage in the precorneal region, low penetration through the cornea, and a high frequency of application that decreases bioavailability to less than 5 % (Greaves and Wilson, 1993; Kuno and Fujii, 2011; Thrimawithana et al., 2011).

Prednisolone (PRED) ophthalmic solution 1 % is available in the market as eye drops. Unfortunately, it suffers from low contact time with cornea causing rapid drainage which results in low bioavailability of the drug. This could enhance the frequency of drug application and decrease patient compliance, which is considered as a communal disadvantage of topical ocular drug delivery systems. PRED was previously loaded into niosomes (Gaafar et al., 2014) and nanocapsules (Katzer et al., 2014) in an attempt to improve its ocular delivery.

Nano-scaled colloidal drug delivery systems were found to be effective in overcoming the imperfections related to topically applied PRED solution. They have advantages like high bioavailability, sustained drug release and effective drug delivery to the target sites (Bucolo et al., 2012; Greaves and Wilson, 1993; Kuno and Fujii, 2011; Sahoo et al., 2008). Spanlastics (SPLs) are very elastic surfactant-based nano-carrier systems developed by Kakkar and Kaur (Kakkar and Kaur, 2011). Non-ionic surfactants (Span 60 and Span 80) and an edge activator (EA) are the major components of spanlastics. Spanlastics are biodegradable nanovesicles that are non-immunogenic and nontoxic. In addition, they

are more chemically stable than normal liposomes (Zaki et al., 2022b). Spanlastics, like niosomes, have advantages because they are osmotically active, they have chemical stability, extended storage period, good patient compliance, and easy access to raw materials (Liu et al., 2019), and they can also improve corneal permeability. Because of these factors, numerous studies are being conducted to investigate the usage of SPLs formulations as a viable delivery approach over traditional nanovesicles. A lot of research has been done regarding the use of spanlastics for the ocular delivery of many drugs like travoprost (Shukr et al., 2022), clotrimazole (Abdelbari et al., 2021), and cyclosporine (Liu et al., 2019). On the other hand, SPLs are disadvantaged by poor mucoadhesion characteristics due to their surface negative charge which results in difficulty in absorption to the ocular surface which is electronegative (Liu et al., 2019).

Many efforts were taken to improve ocular drug bioavailability, including lengthening the time of contact between the drug and the eye and utilizing viscolyzers to enhance the viscosity of the formulations, but only a minor increase in retention time was observed (Grassiri et al., 2021).

High viscosity ointments and gels, on the other hand, extended contact time with the eye but caused impaired vision, a sticky sensation, and reflex blinking as a result of the irritating impact (Said et al., 2024).

Mucoadhesive polymers that adhere to the outer mucous layer surrounding the eye surface are another option for increasing ocular medication absorption (Grassiri et al., 2021). The use of solid dosage forms such as films or inserts permitted a sustained release effect of the drug with a low frequency of administration (Said et al., 2024), but they have drawbacks such as foreign body sensation, irritation caused by their movement around on the ocular surface, and the need to manually remove insoluble inserts because they are not biodegraded, such as Ocusert, Akorn, Buffalo Grove, and IL. Because of these concerns, solid dose forms are not extensively used in ocular therapy (Said et al., 2024).

Sponges are ocular soluble inserts which revealed excellent results in controlling the delivery of drugs (Said et al., 2024). They have a three-dimensional structure created by cross linking polymers. They are prepared by lyophilization which results in dispersing air in a solid matrix. This resulted in embedding the drug in a sponge-like hydrophilic polymer matrix (Said et al., 2024). Sponges are new candidates that have many advantages like easy preparation technique and minimized foreign body sensation in comparison to other ocular solid dosage forms, as the sponge-like nature leads to rapid hydration and gelation in the eye (Said et al., 2024). Moreover, mucoadhesive sponges have demonstrated benefits in maintaining their swollen gel structure for an extended period of time, allowing for a longer residence time and more efficient medication absorption (Khafagy et al., 2022). However, little research has been published concerning the use of sponges as an ocular drug delivery systems, like sponge-like acyclovir ocular minitables (Refai and Tag, 2011), levofloxacin hemihydrate ocular semi-sponges (Sahar et al., 2016) and voriconazole ocular spongy like insert (Said et al., 2024).

Chitosan is a natural biocompatible, biodegradable, and mucoadhesive cationic polysaccharide (Han et al., 2012; Wang et al., 2011). It possesses a positive charge at physiological pH (7.4), which initiates an electrostatic interaction with the negative charge of the mucin coating the cornea, improving corneal retention (Wang et al., 2011). Furthermore, it exhibits penetration-enhancing characteristics due to the transitory opening of tight connections between corneal cells (Alonso and Sánchez, 2003; Ibrahim et al., 2016; Janagam et al., 2017). It also possesses anti-inflammatory, antioxidant, anticancer and antimicrobial activities (Kim, 2018).

This study is meant to formulate PRED as a mucoadhesive and biodegradable spanlastics loaded cationic spongy insert to increase the drug penetration into the eye tissue, increase the residence time of the drug in the eye, sustain the drug release in a controlled manner which reduces the number of instillations in the eye, reduce the foreign body sensation caused by other ocular solid dosage forms, improve the

**Table 1**

I-optimal Design for optimization of PRED loaded SPLs.

Independent variable.	Levels	
	Low	High
Sonication time (X1)	4	12
Span60: EA ratio (X2)	1:1	6:1
Type of EA(X3)	Tween 80	PVA

Dependent variables	R2	Adjusted R2	Predicted R2	Constraints	Adequate precision
EE% (Y1)	0.9984	0.9980	0.9973	Maximize	154.2044
Vesicles size (nm) (Y2)	0.9965	0.9937	0.9772	Minimize	52.9862
Absolute zeta potential (mV) (Y3)	0.8314	0.7893	0.6972	Maximize	10.1908

stability of the formulation, deliver more accurate doses than conventional eye drops, and hence, increasing the patient compliance and therapy outcomes.

## 2. Materials and methods

### 2.1. Materials

Prednisolone Na phosphate (PRED) was kindly gifted by Al jazeera Company for pharmaceuticals. Methanol, chloroform, Span60, Tween 80, Polyvinyl alcohol (PVA) (M.wt 115,000, 25–32 cps, degree of polymerization 1700–1800), and chitosan (high molecular weight 310,000–375,000 Da, 800–2000 cps) were all purchased from Sigma Aldrich (St. Louis, MO, USA). Xylazine hydrochloride 2 % (Xyla ject®; ADWIA, Egypt). Ketamine hydrochloride 5 % (Keiran; EIMC pharmaceuticals Co., Egypt). *Escherichia coli* (Sigma-Aldrich, Co., Egypt). Fluorescein staining (Bio-Glo® Fluorescein sodium Strips 1 mg; HUB pharmaceuticals, LLC., USA). Sodium thiopental 500 mg (Anapental® 500 mg vial; Sigma tec., Egypt). Primary anti-HSP90 antibody (Proteintech, Germany). Endogenous peroxidases and HRP-labelled secondary detection kit (BioSB, USA).

**Table 2**

Output data of I-optimal Design for optimization of PRED-loaded SPLs.

Formula code	Independent variables			Dependent variables			PDI
	Sonication time (X1)	Span60: EA ratio (X2)	Type of EA (X3)	EE% (Y1)	Vesicles size (nm) (Y2)	Zeta potential (mV) (Y3)	
SPLs 1	6.16	4:1	Tween 80	80.62 ± 2.12	184.67 ± 3.25	-32.4 ± 0.23	0.212 ± 0.09
SPLs 2	4	4:1	PVA	75.3 ± 1.87	280.45 ± 6.54	-31.5 ± 0.18	0.354 ± 0.13
SPLs 3	9.84	4:1	PVA	73.2 ± 2.17	275.23 ± 7.83	-33.4 ± 0.15	0.124 ± 0.28
SPLs 4	9.8	6:1	Tween 80	85.7 ± 0.89	150.63 ± 5.73	-36.2 ± 0.41	0.473 ± 0.14
SPLs 5	4	6:1	PVA	80.6 ± 1.74	250.4 ± 7.73	-38.6 ± 0.20	0.187 ± 0.24
SPLs 6	4.6	1:1	PVA	66.12 ± 3.21	292.6 ± 4.38	-30.4 ± 0.32	0.498 ± 0.08
SPLs 7	4	6:1	Tween 80	87.3 ± 2.81	154.8 ± 2.81	-34.2 ± 0.57	0.164 ± 0.24
SPLs 8	11.4	1:1	PVA	63.8 ± 1.83	284.7 ± 6.98	-29.5 ± 0.24	0.504 ± 0.05
SPLs 9	8	1:1	Tween 80	71.4 ± 2.76	205.34 ± 8.32	-28.6 ± 0.30	0.283 ± 0.20
SPLs 10	6.88	4:1	PVA	74.6 ± 3.04	275.3 ± 4.62	-32.7 ± 0.12	0.562 ± 0.07
SPLs 11	6.16	4:1	Tween 80	80.5 ± 1.89	180.45 ± 5.48	-35.2 ± 0.09	0.153 ± 0.22
SPLs 12	9.8	6:1	Tween 80	85.3 ± 1.54	145.8 ± 6.24	-35.6 ± 0.33	0.194 ± 0.11
SPLs 13	12	1:1	Tween 80	70.6 ± 2.67	185.4 ± 4.82	-30.2 ± 0.72	0.336 ± 0.03
SPLs 14	12	4:1	Tween 80	78.7 ± 0.83	163.8 ± 8.83	-34.8 ± 0.58	0.456 ± 0.14
SPLs 15	9.84	4:1	PVA	72.8 ± 0.95	271.6 ± 7.87	-33.2 ± 0.21	0.273 ± 0.16
SPLs 16	9.12	6:1	PVA	78.8 ± 1.58	240.3 ± 10.42	-36.7 ± 0.60	0.263 ± 0.41
SPLs 17	12	6:1	PVA	78.2 ± 2.85	234.12 ± 9.64	-35.8 ± 0.48	0.382 ± 0.02
SPLs 18	4.6	1:1	PVA	66.4 ± 3.11	293.8 ± 8.88	-27.1 ± 0.14	0.472 ± 0.18
SPLs 19	4	1:1	Tween 80	72.3 ± 1.63	222.7 ± 6.99	-29.8 ± 0.36	0.511 ± 0.11
SPLs 20	11.4	1:1	PVA	64.1 ± 2.73	285.3 ± 5.43	-25.3 ± 0.81	0.342 ± 0.19
SPLs 21	6.2	6:1	PVA	79.6 ± 0.93	246.6 ± 7.11	-37.2 ± 0.08	0.291 ± 0.33

PVA: Poly vinyl alcohol; EA: edge activator; PDI: poly dispersity index; EE%: the percentage of entrapment efficiency. Data are shown as mean ± SD (n = 3).

### 2.2. Statistical design of PRED Loaded SPLs

The influence of different formulation variables on the entrapment efficiency (EE%) (Y1), Vesicles' size (VS) (Y2), and Zeta potential (ZP) (Y3) of PRED loaded SPLs was studied using an I-optimal design. Stat-Ease's Design Expert® software (Ver. 12, Minneapolis, Minnesota, USA) was used. The sonication time (X1) ranged between 4 and 12 min, the Span 60: EA ratio (X2) was between 1:1 and 6:1, and the type of edge activator (X3) was either tween 80 or PVA. The PRED concentration was kept constant in all formulations at 100 mg/10 ml. This yielded 21 experimental runs. The formulation variables (low and high level) and dependent responses are shown in Table 1. The composition of PRED-loaded SPLs is shown in Table 2.

### 2.3. Preparation of PRED loaded SPLs

Ethanol injection method was used to prepare PRED SPLs with minor modifications (Zaki et al., 2022b). Span 60 was used as the surfactant while Tween 80 and PVA were used as the edge activators. The ratio of spans 60 to EA was varied between 1:1 to 6:1, as shown in Table 1. Each formula contains 100 mg PRED. In brief, the weighed amounts of span 60 and PRED were dissolved in a 5 ml organic phase composed of a mixture of chloroform: methanol in a ratio of 2:1 (v/v) while the edge activator was dissolved in 10 ml aqueous phase. The organic phase was then slowly injected into the aqueous phase heated at 50 °C while stirring at 1000 rpm for 1 h. A white milky suspension of PRED-loaded SPLs was formed. The formed SPLs were then sonicated for a time as indicated in Table 2.

### 2.4. Characterization of PRED-Loaded SPLs

#### 2.4.1. Determination of entrapment efficiency (EE%)

Centrifugation at 17000 rpm for 1 h at 4 °C using a cooling centrifuge (SIGMA 3–30 K, Sigma, Steinheim, Germany) separated PRED-loaded SPLs from the free drug (Zaki et al., 2022a; Zaki et al., 2022c). After diluting the supernatant, PRED in the supernatant was quantified using a UV spectrophotometer (Shimadzu UV-1800, Kyoto 604–8511, Japan). The measurements were done at  $\lambda_{max}$  (242 nm). Within the concentration range of 6–30 µg/ml, the technique was validated for linearity (R2 = 0.9999).

The EE% was calculated using the equation below (Zaki et al., 2022c):

$$EE\% = \frac{TD - FD}{TD} \times 100 \quad (1)$$

Where FD represents the amount of free drug, TD represents the total amount of drug, and EE% represents the percentage of entrapment efficiency.

#### 2.4.2. Determination of vesicle size (VS), polydispersity index (PDI), and zeta potential (ZP)

A Zetasizer (Malvern Instruments, Worcestershire, UK) was used to measure the VS, PDI, and ZP values. The measurements were carried out at 25 degrees Celsius after appropriate dilutions with distilled water (Zaki et al., 2022a). All measurements were done three times.

#### 2.5. Statistical analysis, optimization, and validation

Using the Design Expert® software, a statistical factorial analysis of variance (ANOVA) was done to determine statistical significance on the observed responses. The optimized formula with the highest EE% and ZP and the least VS was chosen using a desirability function. Following that, it was prepared and evaluated in relation to EE%, VS, and ZP to determine the validity of the used statistical models. The relative errors in percentage between the expected values and the obtained findings were then determined (Mazyed and Abdelaziz, 2020; Zaki et al., 2022c):

$$\%Relative\ error = \frac{values\ predicted - obtained\ findings}{values\ predicted} \times 100 \quad (2)$$

#### 2.6. Evaluation of the optimum PRED loaded SPLs

##### 2.6.1. Transmission electron microscopy (TEM)

The morphology of the optimized SPLs formulation was visualized using a transmission electron microscope (TEM; JEOL JEM-1010, Tokyo, Japan). Samples were diluted and deposited on a carbon-coated copper grid for this purpose. They were then coated with 2 % (w/v) phosphotungstic acid, air dried for 5 min, and visualized using a TEM at room temperature with a magnification power of x80000 and an acceleration voltage of 80 KV (Salem et al., 2021).

##### 2.6.2. Study of in-vitro release

The release of PRED from the optimized PRED-loaded SPLs formula was compared to the drug solution by inserting the equivalent to 5 mg PRED from each within the dialysis bags (mw cut-off 12 kDa; Sigma Aldrich). Following that, both were suspended in a 250 ml of dissolution media (phosphate buffer pH (6.4)) (Hosseinzadeh et al., 2012; Kantaria et al., 2023) in a dissolution apparatus (Pharm Test, Hainburg, Germany) with the temperature set at 37 °C and the stirring set at 100 rpm. The dissolution media was then sampled at various intervals of 1, 2, 3, 4, 5, and 6 h, and an equivalent volume of fresh media was immediately added. The PRED concentration in the collected samples was then determined using a UV spectrophotometer. The subsequent equation was used to calculate the percentage of PRED released at different time points (Zaki et al., 2022a):

$$Q_n = \frac{C_n \times V_r + \sum_{i=1}^{n-1} C_i \times V_s}{initial\ drug\ content} \quad (3)$$

Where,

Q<sub>n</sub>: Collective percentage of PRED released.

C<sub>n</sub>: PRED concentration at the n<sup>th</sup> sample in the dissolution medium.

V<sub>r</sub>: The volume of the dissolution medium.

V<sub>s</sub>: The sample volume.

$\sum_{i=1}^{n-1} C_i$ : The overall of the beforehand determined concentrations.

To establish the release profile of the optimum PRED-loaded SPLs formula in contrast to the drug solution, a plot of the proportion of PRED

released (Q<sub>n</sub>) at various time points vs. the relevant time was generated.

##### 2.6.3. Studying the aging effect

The optimum PRED-loaded SPLs formula stability was assessed at various time intervals in terms of EE%, VS, and ZP after thirty days in an airtight container kept away from light at 4 °C (Zaki et al., 2022a).

#### 2.7. Preparation of optimum PRED loaded SPLs mucoadhesive spongy insert (SPLs-SI)

The SPLs-SI were prepared using the casting/freeze-drying process (Said et al., 2024). Briefly, 1 % chitosan is dissolved in 1 % (v/v) acetic acid solution followed by addition of the optimum SPLs formula while stirring on a magnetic stirrer. The equivalent to 1 mg PRED from the mixture was poured into PVC blister pockets with a thickness of 4 mm and an interior diameter of 8 mm. The blisters were then placed in a freezer at -18 °C for 24 h. The samples were then lyophilized in a freeze dryer at -45 °C and a vacuum of 7 × 10<sup>-2</sup> mbar. The prepared SPLs-SI were stored in a desiccator until use.

#### 2.8. Assessment of optimum PRED loaded SPLs-SI

##### 2.8.1. Visual appearance

The colour and texture of the lyophilized formulations were assessed visually.

##### 2.8.2. Surface pH

The SPLs-SI was allowed to swell for 2 h at room temperature by being in touch with 2 ml of STF. The pH was determined by placing a pH strip in contact with its surface and allowing it to equilibrate for 1 min (Saher et al., 2016).

##### 2.8.3. Study of the mucoadhesion

Mucoadhesion was measured using the Bertram and Bodmeier displacement method (Bertram and Bodmeier, 2006). Agar/mucin solutions (1 % and 2 % w/w, respectively) in STF were prepared by first dissolving agar in hot simulated tear fluid (STF), then allowing the solution to cool a bit before adding mucin to the warm agar solution while stirring until dissolved. The Agar/mucin solution was then put into a petri dish and refrigerated at 4-8 °C for 2 h to allow a gel to develop. The SPLs-SI was placed on top of the agar/mucin gel. The Petri plates were flipped vertically and placed in a 37 °C incubator. The SPLs-SI was shifted downward due to the gravity impact. After 1 h, the distance moved by the SPLs-SI was measured in centimeters (n = 2). The distance travelled by the SPLs-SI was inversely related to their mucoadhesive power (Said et al., 2024).

##### 2.8.4. Fourier-transform infrared (FTIR) spectroscopy

FTIR spectra were made for PRED, the optimum SPLs formula and the optimum PRED loaded SPLs-SI. Dry potassium bromide was mixed with nearly 2-3 mg of each sample and squashed into a disc before being scanned at 4000-500 cm<sup>-1</sup> at room temperature.

##### 2.8.5. Differential scanning calorimetry (DSC)

DSC analysis was done for PRED, the optimum SPLs formula and the optimum PRED loaded SPLs-SI. Differential scanning calorimeter ((DSC N-650; Scinco, Italy)) was used to perform DSC studies by placing about 5 mg sample in its aluminum pan followed by heating at a rate of 10 °C/min, in a dry nitrogen atmosphere to 300 °C.

##### 2.8.6. Study of X-ray diffraction (XRD)

The scanning of the X-ray diffraction patterns of PRED, the optimum SPLs formula and the optimum PRED loaded SPLs-SI was done at 10°/min speed rate and 0-60° range (2θ) using an Ultima IV Diffractometer (Rigaku Inc. Tokyo, Japan College of Pharmacy, King Saud University, Riyadh, KSA).

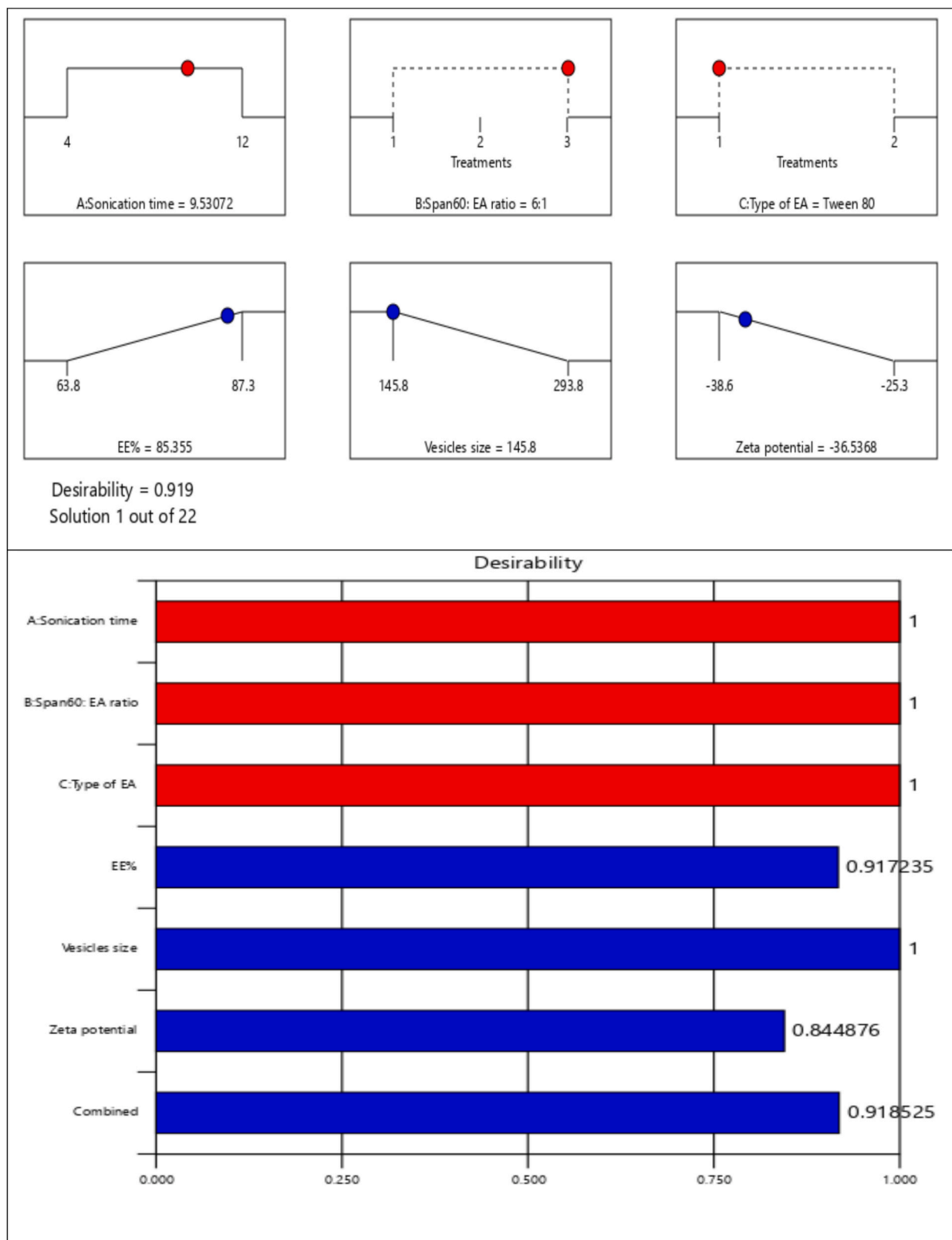


Fig. 1. Desirability and numerical optimization for PRED loaded SPLs using I- optimal design.

## 2.9. In-vivo studies

### 2.9.1. Animals

Animal procedures were approved by the Research Ethics Committee for experimental and clinical studies at the Faculty of Pharmacy, Cairo

University, Egypt (Approval no. PI3413) following with the local and national regulatory standards set for animal care by the animal care committee at Cairo University.

The study was carried out on twelve New Zealand male white rabbits. All rabbits enrolled in this study were obtained from the animal

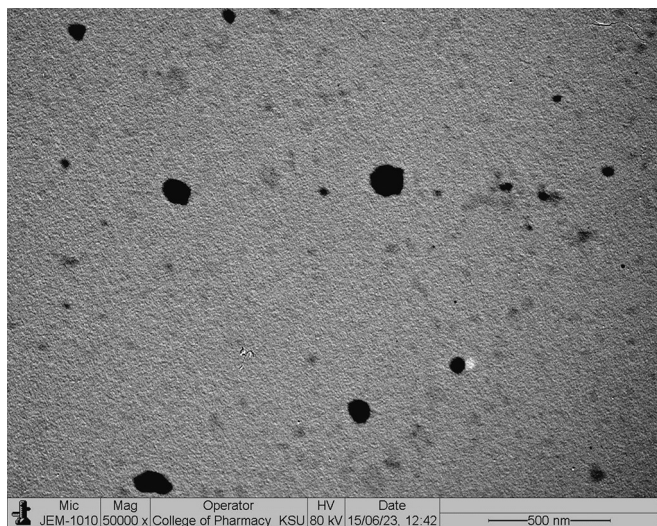
**Table 3**

The expected responses of the optimized formula and its validation.

The optimized formula	Independent variables			Predicted Responses			Desirability
	Sonication time (X1)	Span60: EA ratio (X2)	Type of EA (X3)	EE%	Vesicles size	Zeta potential	
	9.53072	6:1	Tween 80	85.355	145.8	-36.5368	0.919

Validation of the optimum formula			
Responses	Predicted value	Experimental value	% Relative error
EE%	85.355	87.56	2.583
Vesicles size	145.8	152.2	4.389
Zeta potential	-36.5368	-37.38	2.307



**Fig. 2.** TEM image of the optimum SPLs formulation.

house of the Giza memorial institute for ophthalmic research, Egypt. All animals were housed two to three rabbits per cage at a central temperature of 22–25 °C with 12 h light/12 h dark cycle and fed on a laboratory balanced diet. All procedures were conducted according to the principles enunciated in the guide for care and use of laboratory animals. All rabbits enrolled in this study underwent a complete clinical, physical and ophthalmological examination by a qualified veterinary ophthalmologist (KMA) to ensure that they were completely healthy and free from any infectious, contagious or ophthalmic diseases.

The rabbits were classified and divided randomly into four groups of three rabbits each (six eyes/group) according to the following:

1. Group I: Prednisolone loaded spanlastics spongy insert (G-SPLs-SI)
2. Group II: Prednisolone loaded spanlastics (G-SPLs)
3. Group III: Commercial prednisolone eye drops (G-OPT)
4. Group IV: Control group (G-CO)

**2.9.2. Induction of uveitis and study design**

An experimental uveitis was induced in both eyes of all rabbits enrolled in this study through intracameral injection of endotoxin (Fig. 1 a and b). Before induction, the rabbits received an intramuscular injection of xylazine hydrochloride 2 % (Xyla ject®; ADWIA, Egypt) in a dose of 1 mg/kg *b.w.*, and anesthetized with ketamine hydrochloride 5 % (Keiran; EIMC pharmaceuticals Co., Egypt) in a dose of 20 mg/kg. The endotoxin used to induce uveitis was lipopolysaccharide (LPS) from *Escherichia coli* (Sigma-Aldrich, Co., Egypt). The rabbits were re-examined 24 h after the endotoxin injection for clinical signs of uveitis and received the treatment according to the study design as follows:

**G-SPLs-SI:** The rabbits in this group were treated using prednisolone loaded spanlastics spongy insert that was applied once daily to the lower cul-de-sac of both eyes.

**G-SPLs:** The rabbits in this group were treated using prednisolone loaded spanlastics that was instilled once daily in the lower cul-de-sac of both eyes.

**G-OPT:** The rabbits in this group were treated using prednisolone acetate 1 % eye drops (Optipred™ eye drops; Jamjoom pharmaceuticals, Jeddah - Saudi Arabia) 4 times a day.

**G-CO:** The rabbits in the control group received no treatment.

**Table 4**

Stability study for the optimized formula for 30 days at 4 °C.

Responses	Fresh	After 7 days	After 30 days
EE%	87.56 ± 2.04	87.23 ± 0.86	86.74 ± 1.72
Vesicles size (nm)	152.2 ± 5.12	151.91 ± 7.63	151.23 ± 8.53
Zeta potential (mV)	-37.38 ± 0.34	-37.15 ± 1.03	-36.67 ± 0.74

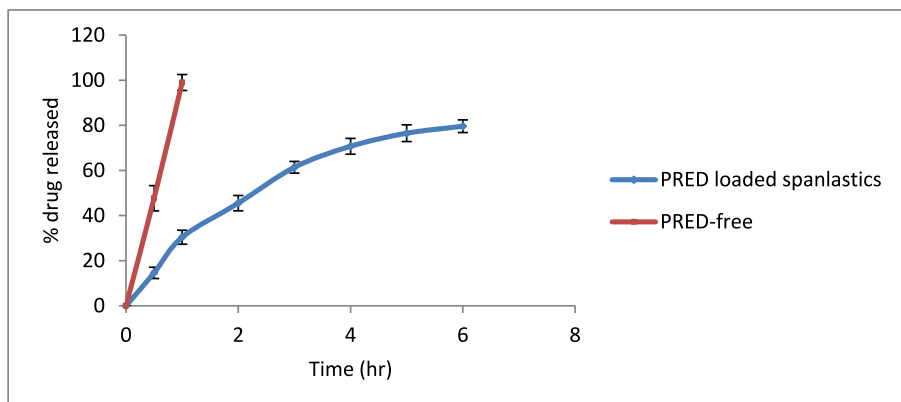


**Fig. 3.** In-vitro drug release profile of PRED loaded spanlastics optimum formula compared to free PRED.

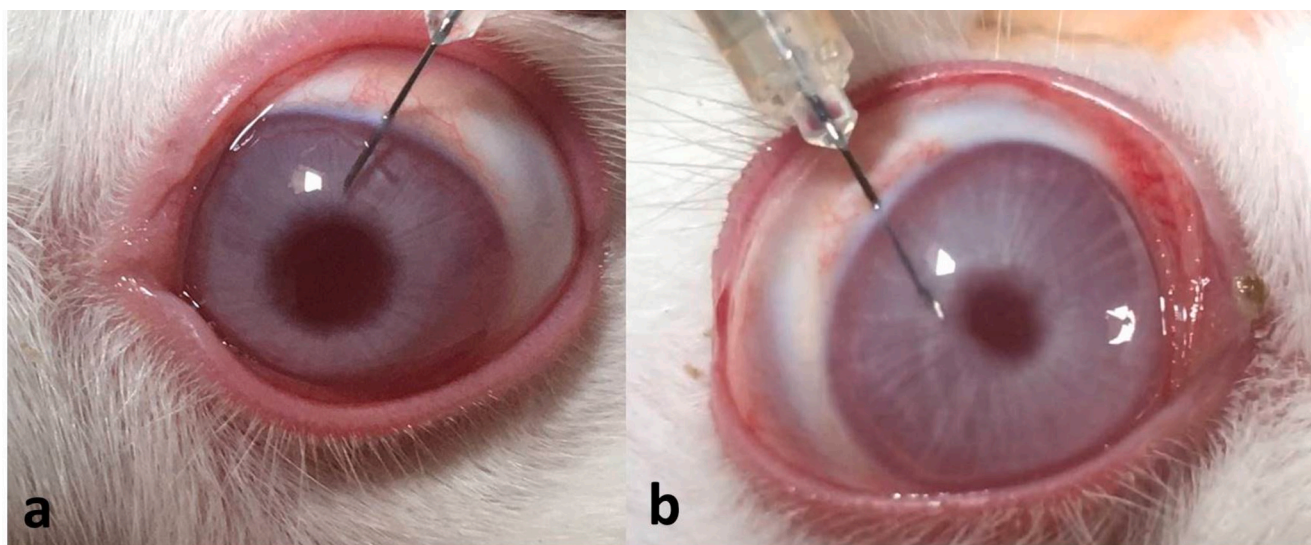


Fig. 4. a and b. Induction of uveitis through intracameral injection of lipopolysaccharide (LPS) from *Escherichia coli*.

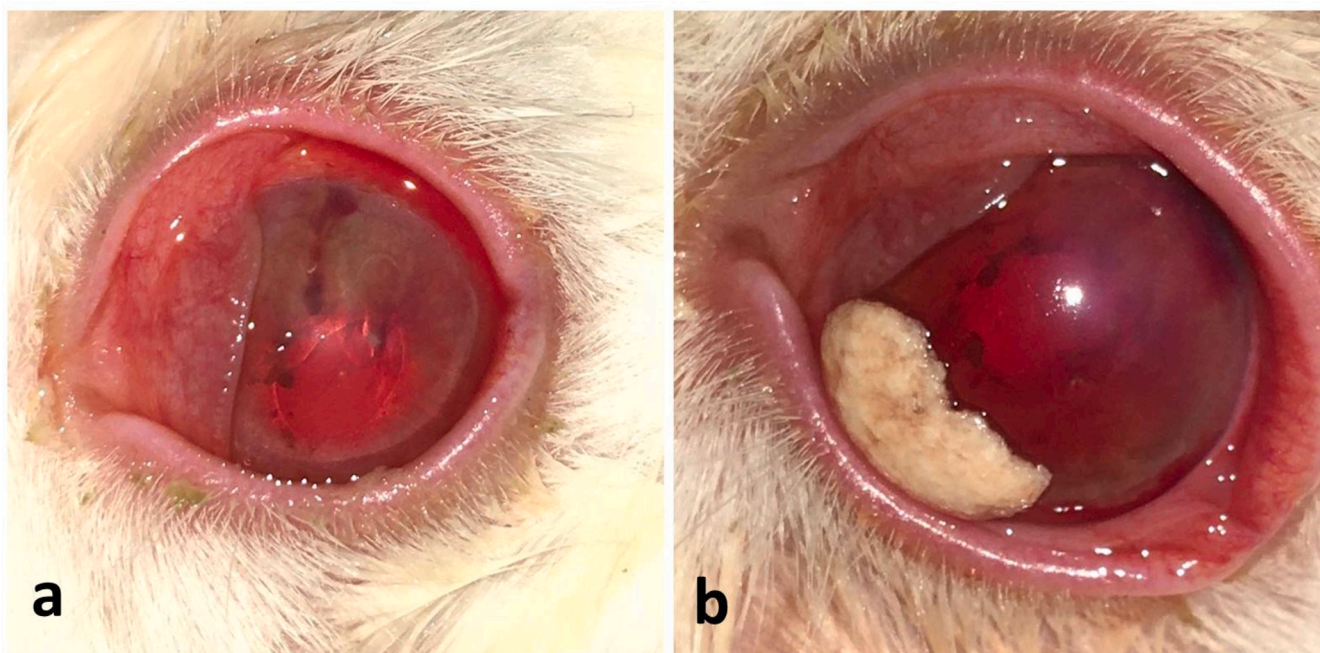


Fig. 5. (a) Showing the clinical signs of uveitis after 24 h from induction. (b) Successful application of the prednisolone loaded spanlastics spongy insert in the G-SPLS-SI group.

The treatment was continued for two weeks after induction of uveitis. During the period of the study design the rabbits were evaluated daily by complete ophthalmological examination that aimed at grading of uveitis and evaluation of the clinical signs.

#### 2.9.3. Ophthalmological examination and evaluation of uveitis

The ophthalmic examination included: slit lamp examination (SL 14 handheld slit lamp, Kowa, Tokyo, Japan), fluorescein staining (Bio-Glo® Fluorescein sodium Strips 1 mg; HUB pharmaceuticals, LLC., USA) Schiötz tonometry (Riester, Germany) and indirect ophthalmoscopy (Riester, Germany). The standard protocol for the vision assessment was used via evaluation of the menace response, dazzle reflex, direct, and consensual pupillary light reflexes (Maggs et al., 2017). The clinical signs of ocular inflammation were graded on a scale of 0 to 4 according to the scoring system described by Ruiz-Moreno et al.,1992 (Ruiz-

Moreno et al., 1992). The clinical inflammatory features included: conjunctival hyperemia, congestion of episcleral and limbal blood vessels, corneal edema, hyphema, aqueous flare and iris neovascularization of uveitis were graded from a score of 0 to 4 by a blinded observer depending on the severity of each clinical symptom as follow: 0: None or absent, 1: Discrete, 2: Mild, 3: Moderate, 4: Severe. Grading of the clinical signs and vision assessment was reported at 48 h, 5 days, 7 days, 10 days and 14 days from the start of treatment for all rabbits enrolled in the present study.

#### 2.9.4. Histopathologic examination

At the end of the experiment, the rabbits' eyes were enucleated after being euthanized using intravenous injection of sodium thiopental 500 mg (Anapental® 500 mg vial; Sigma tec., Egypt) (Weichbrod et al., 2018). Tissues were fixed in 10 % formalin and processed to obtain

**Table 5**

Clinical signs and scores of uveitis observed at the evaluation periods in this study.

Clinical signs of uveitis	Period of evaluation	G-SPLs-SI	G-SPLs	G-OPT	G-CO	
Conjunctival hyperemia	48 h	4	4	4	4	
	5 days	4	4	4	4	
	7 days	3 ± 1.15	3.33 ± 0.74	3.5 ± 0.5	3.83 ± 0.37	
		1.6 ± 0.47	2.16 ± 0.37	2.5 ± 0.5	3.66 ± 0.47	
	10 days	1.6 ± 0.47	2.16 ± 0.37	2.5 ± 0.5	3.66 ± 0.47	
		0.33 ± 0.47	0.83 ± 0.68	2	3.33 ± 0.47	
	14 days	0.33 ± 0.47	0.83 ± 0.68	2	3.33 ± 0.47	
		48 h	4	4	4	4
	Congestion of episcleral and limbal blood vessels	5 days	4	4	4	4
		7 days	3 ± 1.15	3.33 ± 0.74	3.5 ± 0.5	3.83 ± 0.37
			1.6 ± 0.47	2.16 ± 0.37	2.5 ± 0.5	3.66 ± 0.47
		10 days	1.6 ± 0.47	2.16 ± 0.37	2.5 ± 0.5	3.66 ± 0.47
			0.33 ± 0.47	0.83 ± 0.68	2	3.33 ± 0.47
		14 days	0.33 ± 0.47	0.83 ± 0.68	2	3.33 ± 0.47
48 h			0	0	0	0
Corneal edema		5 days	3.5 ± 0.5	3.66 ± 0.47	3.83 ± 0.37	3.83 ± 0.37
		7 days	2.66 ± 0.94	3 ± 0.57	3.33 ± 0.47	3.83 ± 0.37
			1.83 ± 0.37	2 ± 0.57	3	3.83 ± 0.37
		10 days	1.83 ± 0.37	2 ± 0.57	3	3.83 ± 0.37
			0.3 ± 0.47	0.83 ± 0.68	1.83	3.33 ± 0.74
		14 days	0.3 ± 0.47	0.83 ± 0.68	1.83	3.33 ± 0.74
			48 h	4	4	4
	Hyphema	5 days	3	3	3	3
		7 days	1.66 ± 0.74	2.33 ± 0.47	2.33 ± 0.47	3 ± 0.47
			0.5 ± 0.76	0.83 ± 0.68	1 ± 0.57	2.33 ± 0.47
		10 days	0.5 ± 0.76	0.83 ± 0.68	1 ± 0.57	2.33 ± 0.47
			0	0.16	0.33	0.83
		14 days	0	0.16	0.33	0.83
			48 h	0	0	0
Aqueous flare		5 days	1.5 ± 0.5	1.66 ± 0.74	1.66 ± 0.74	3 ± 0.47
		7 days	1.16 ± 0.37	1.5 ± 0.5	2.33 ± 0.47	3 ± 0.47
			0.16 ± 0.37	0.83 ± 0.68	1 ± 0.57	2.33 ± 0.47
		10 days	0.16 ± 0.37	0.83 ± 0.68	1 ± 0.57	2.33 ± 0.47
			0	0.16	0.33	2.33
		14 days	0	0.16	0.33	2.33
			48 h	4	4	4
	Iris neovascularization	5 days	1.5 ± 0.5	1.5 ± 0.5	1.66 ± 0.74	3.16 ± 0.37
		7 days	1.16 ± 0.37	1.5 ± 0.5	1.5 ± 0.5	3 ± 0.37
			0.16 ± 0.37	0.66 ± 0.47	1 ± 0.57	3.16 ± 0.37
		10 days	0.16 ± 0.37	0.66 ± 0.47	1 ± 0.57	3.16 ± 0.37
			0	0.16	0.33	3 ± 0.57
		14 days	0	0.16	0.33	3 ± 0.57
			48 h	4	4	4

paraffin blocks. After fixation the tissue was processed in alcohols grades, xylenes changes and finally embedded in paraffin wax. Five µm sections were cut and stained with hematoxylin and eosin (H&E) for light microscopy (Bancroft and Gamble, 2008). Leica DM4B light digital microscopes (Leica, Germany) connected to Leica DMC 4500 digital camera (Leica, Germany) were used to examine the tissue slides and to capture images.

### 2.9.5. Immuno histochemistry

Five µm sections were mounted into adhesive slides for immune staining. Briefly, the tissue sections were rehydrated with distilled water and subjected to heat induced epitope retrieval then incubated with primary anti-HSP90 antibody (Proteintech, Germany) at a dilution of 1:300 for one hour at room temperature. After washing, tissue slides were blocked for endogenous peroxidases then HRP-labelled secondary detection kit (BioSB, USA) was used as manufacturer instructions to develop the reaction. Positive expression was quantified as mean area percent of positive staining in each experimental group.

### 2.9.6. A macroscopic analysis of the gelling process, mucoadhesive behavior, and biodegradation

This was accomplished through visual observation of the animals to determine the time of gelation of the spongy insert, its mucoadhesiveness by evaluating its presence in the lower cul de sac all over the period of the study without detachment, and its biodegradation behavior by noting the time at which the insert completely disappeared from the lower cul de sac (Said et al., 2024).

### 2.9.7. Ocular irritation test

The safety of the SPLs-SI was evaluated using the ocular Draize test on three New Zealand albino rabbits. Each rabbit had one insert inserted in its right eye, while the left eye received no therapy and served as a control. Using a conventional scoring system, ocular irritation signs such as redness, swelling, cloudiness, edema, and hemorrhage were observed at 1, 2, 3, 4, 5, 6, 7, 8, 9, 10, and 24 h post instillation or insertion (Karn et al., 2014).

## 3. Results and Discussion

### 3.1. Evaluation of PRED-loaded SPLs

#### 3.1.1. Estimation of EE%

Table 2 shows that the EE% of various SPLs formulations ranged from 63.8 ± 1.83 to 87.3 ± 2.81. Fig. S1 depicts the impact of Sonication time (X1), Span 60: EA ratio (X2), and Type of EA (X3) on the EE %.

The linear model suited the EE% data well ( $p$ -value < 0.0001), whereas the lack of fit was not statistically significant ( $p$ -value = 0.1890). The difference between the adjusted and predicted R<sup>2</sup> was less than 0.2, indicating that the model was valid (Said et al., 2021; Zaki et al., 2022a; Zaki et al., 2022c). The results reveal that the model had adequate precision 154.2044, implying that it could work well within the planned area (Said et al., 2017, 2018) as shown in Tables 1 and S1.

The equation below demonstrated how the formulation factors affected the EE%:

$$EE\% = +75.95 - 1.25 \times 1 - 7.67X2a + 0.9932X2b - 3.21 \times 3.$$

The ANOVA analysis in Table S1 shows that all three formulation factors, Sonication time (X1), Span 60: EA ratio (X2), and Type of EA (X3), had a significant effect on the EE% values ( $p$ -values < 0.0001).

Regarding the effect of sonication time on EE%, increasing the sonication time from 4 to 12 mins led to a significant decrease in EE% which could be explained by the decreased vesicle size of the SPLs or the escape of PRED to the outer aqueous surrounding media during breakdown and re-formations of SPLs rather than being encapsulated in the nanovesicles (Ngan et al., 2014). These results comply with those of Zaki et al. (Zaki et al., 2022b) who made a study on the effect of the span 60:EA ratio on

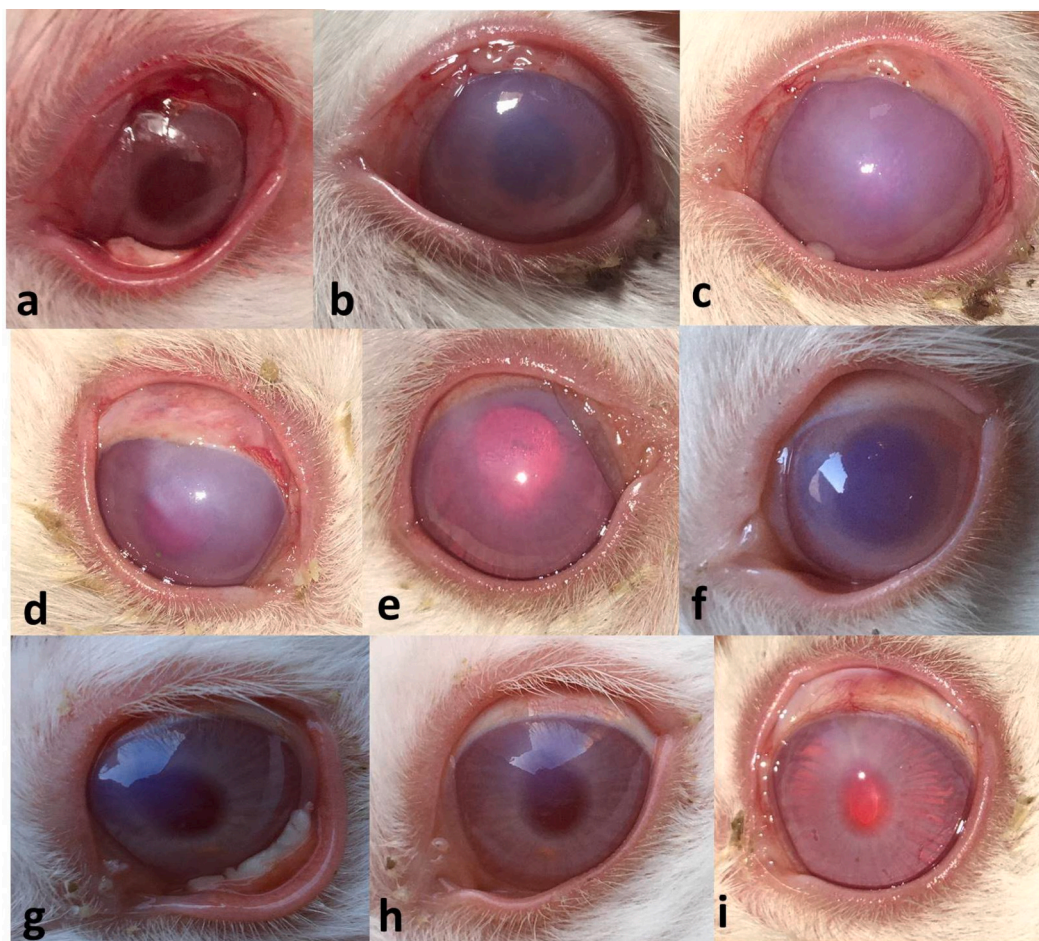


**Fig. 6.** Showing improvement of the clinical signs of uveitis in the G-SPLs-SI group throughout the study periods. (a) Conjunctival hyperemia and intense inflammatory reaction were observed 24 h after induction, (b) corneal edema started to develop afterwards and high grade was observed at day 5 (c). (d, e and f) gradual decrease in the grades of uveitis and corneal edema. (g and h) The clinical appearance at 10th day. (i) A representing eye from G-SPLs-SI group at 14 days showing apparently normal eye.

the EE% of brigatinib loaded SPLs.

In contrast, changing the span 60: EA ratio from 1:1 to 6:1 significantly increased the EE%, probably due to the larger content of span 60, which produced a reduction in fluidization of the SPLs membrane and, as a result, lowered PRED leakage, thereby increasing the EE%. These findings are consistent with those of Badria and Mazyed (Badria and Mazyed, 2020), who studied the effect of the span60:EA ratio on the EE % of (3-Acetyl-11-Keto-Boswellic acid loaded SPLs).

In terms of surfactant type, Tween 80-based SPLs had a greater EE% than PVA-based SPLs. This might be explained by the hydrophilic-lipophilic balance (HLB) of EA, which was 15 for Tween 80 and 18 for PVA, respectively (Foo et al., 2020). As a result of Tween 80 being more hydrophobic than PVA, Tween 80-based SPLs were more stiff by diminishing the amphiphilic property of the vesicles membrane, resulting in a greater EE% (El Zaafarany et al., 2010). These findings are consistent with that of Abdelbari et al. (Abdelbari et al., 2021), who found a greater EE% using Tween 80-based SPLs than pluronic F127-based SPLs for clotrimazole ocular administration.

### 3.1.2. Estimation of VS, PDI and ZP

The VS of different SPLs formulations ranged between  $145.8 \pm 6.24$  and  $293.8 \pm 8.88$  nm as seen in Table 2. The influence of Sonication time (X1), Span 60: EA ratio (X2), and Type of EA (X3) on VS is presented in Fig. S2.

The Two factor interaction model suited the VS data the best (p-value <0.0001). A non-significant lack of fit (p-value 0.0551) and a minor

discrepancy between the adjusted and predicted R2 (difference less than 0.2) confirm the model's validity (Said et al., 2021; Zaki et al., 2022a; Zaki et al., 2022c). As indicated in Tables 1 the adequate precision was 52.9862 (higher than 4), showing that the model could work well within the planned space (Said et al., 2021; Said et al., 2018).

The following equation depicts the effect of formulation factors on VS:

$$VS = +223.02 - 9.15 \times 1 + 23.77X2a + 2.88X2b + 45.97 \times 3 - 1.96X1X2a + 0.4370X1X2b + 3.45X1X3 - 3.66X2aX3 + 3.30X2bX3.$$

ANOVA study (Table S1) revealed that the three formulation factors, Sonication time (X1), Span 60: EA ratio (X2), and Type of EA (X3), significantly influenced the VS values (p-values <0.0001).

Concerning the effect of sonication time on VS, the VS of the SPLs decreased with increasing sonication time which could be related to the passage of pressure produced by the ultrasonic waves through the colloidal formulation which results in particle fraction and consequently the size is reduced (El-Helw and Fahmy, 2015). This observation is in agreement with that of Ghaderi et al. (Ghaderi et al., 2014), who found that there is a reduction in the size of gammaoryzanol nanoparticles with the increase in the sonication time. In another study, Badr-Eldin et al. (Badr-Eldin et al., 2022) reported that there is an inverse relationship between sonication time and the size of simvastatin SPLs.

Regarding the effect of the span 60: EA ratio on VS, it was observed that increasing the ratio from 1:1 to 6:1 led to a significant decrease in VS which could be attributed to reduced concentration of EA in the mixture. Both tween 80 and PVA are hydrophobic non-ionic surfactants

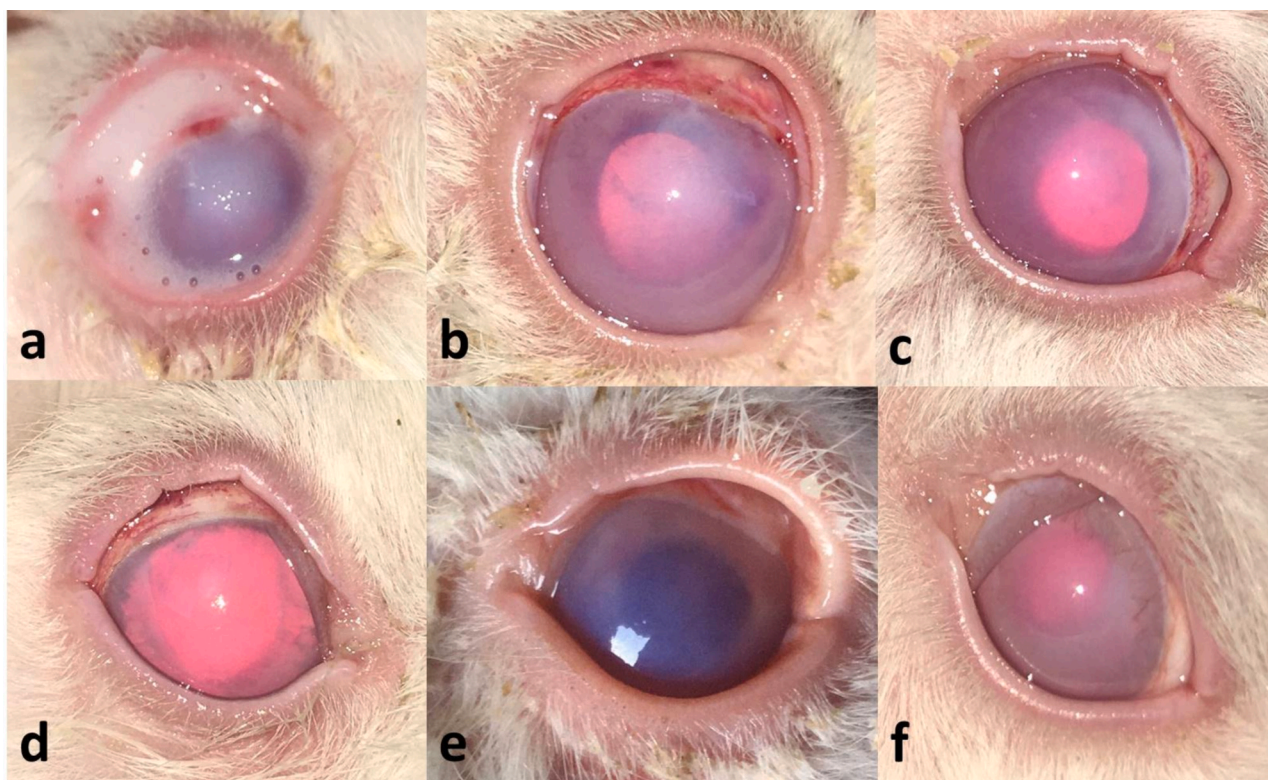


**Fig. 7.** Showing eyes of G-SPLs group; (a) application of prednisolone loaded spanlastics solution and (b) corneal edema, hyphema and congestion of episcleral and limbal blood vessels at 5 days after treatment. (c) A rabbit eye at 7 days post-treatment showing corneal edema and congestion of episcleral and limbal blood vessels. (d and e) photograph at 10 days post treatment showing improvement of the clinical signs of uveitis. (f) A representing image at 14 days post treatment showing apparently normal eye with mild corneal edema.

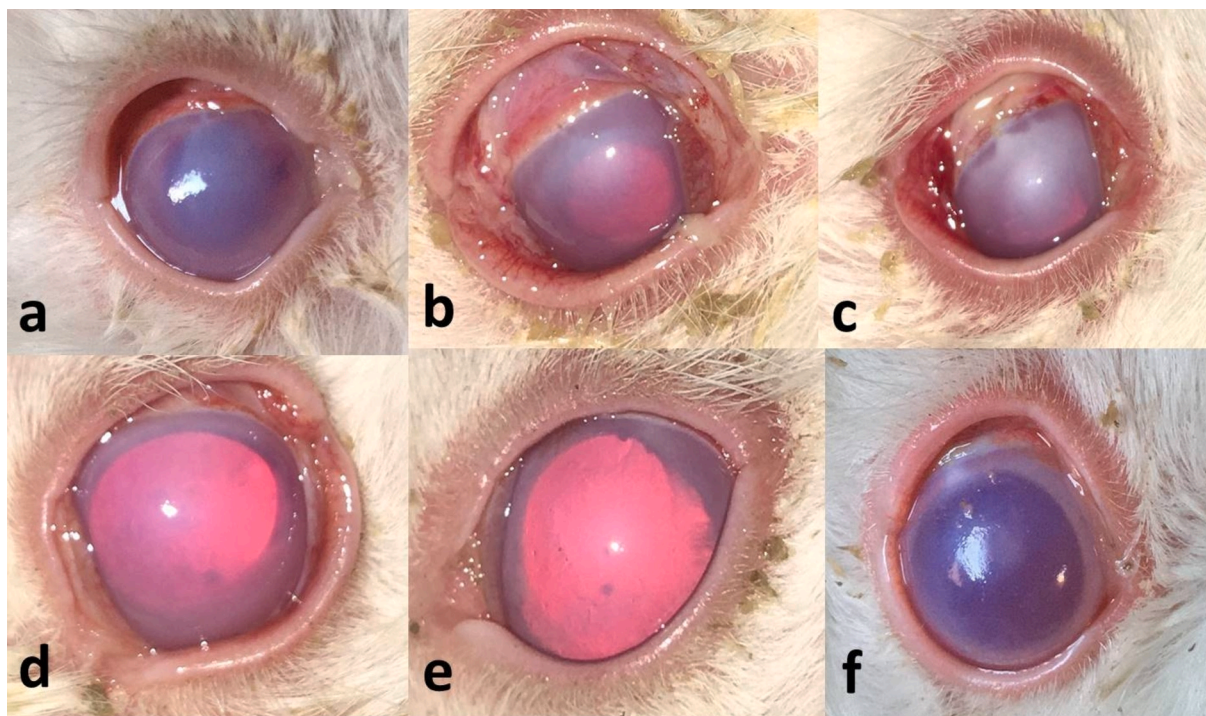


**Fig. 8.** Showing eyes of G-OPT group; higher grades of hyphema (a), Conjunctival hyperemia, congestion of episcleral and limbal blood vessels (b) and corneal edema (c) were observed at 5 days post-treatment. (d and e) representing images at 10 days post-treatment showing improvement of the clinical signs of uveitis. (f) A representing image at 14 days post-treatment showing apparently normal eye with mild corneal edema.

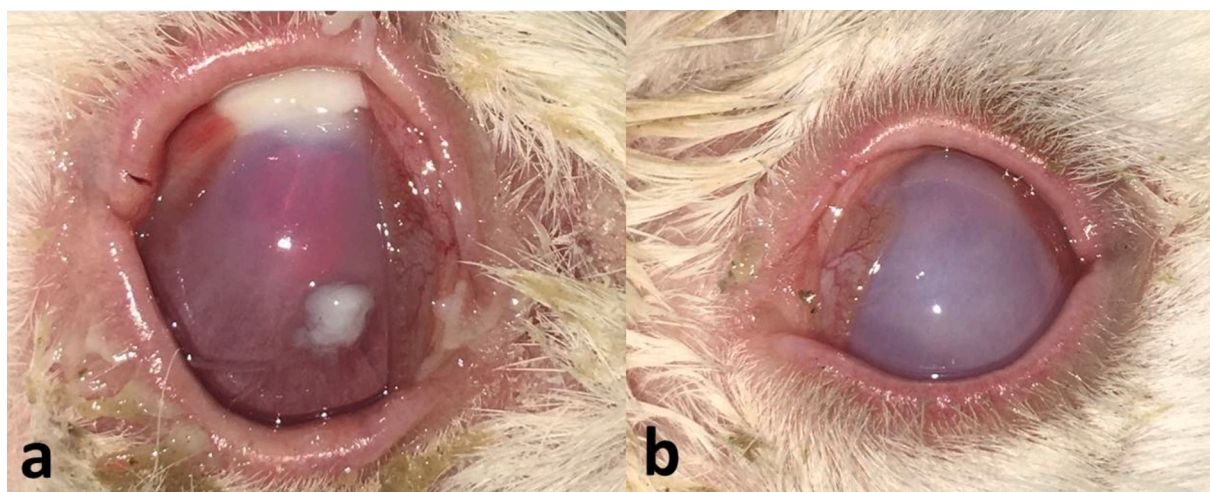


**Fig. 9.** Showing eyes of G-CO group; (a) higher grades of ocular inflammation with mucopurulent discharges at 10 days of the study and severe corneal edema and conjunctivitis at 14 days.

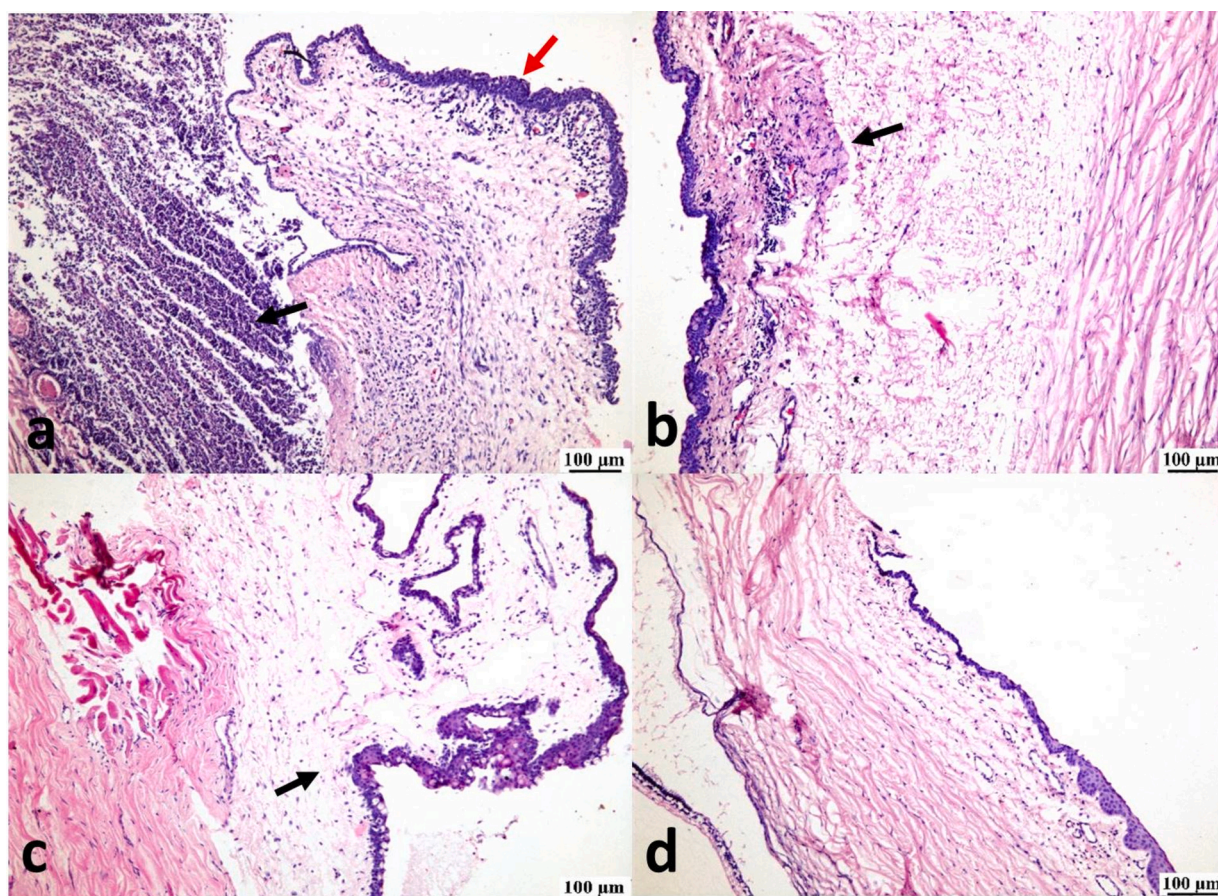


**Fig. 10.** Photomicrograph showing histopathologic evaluation (H&E) of the conjunctiva in the different groups. (a) Showing intense inflammatory cells infiltration (black arrow) and thickened epithelial lining (red arrow) in G-CO group. (b) Moderate inflammatory cells infiltration (arrow) in G-OPT group. (c) Mild inflammatory edema (arrow) in G-SPLs group. (d) Apparently normal conjunctiva in G-SPLs-SI group. (For interpretation of the references to colour in this figure legend, the reader is referred to the web version of this article.)

(Mahmoud et al., 2022). They increased the elasticity of the vesicles by imparting flexibility to the bilayer membrane (Elsaied et al., 2019) which results in increasing the water uptake by the vesicles and hence the VS increase. These results are in agreement with that of Zaki et al. (Zaki et al., 2022b) who reported that increasing the ratio of span 60: EA led to a significant decrease in the size of brigatinib SPLs.

With respect to the effect of EA type on VS, it was found that formulations prepared with PVA were larger in size than those prepared with tween 80. This could be related to the higher HLB value of PVA than tween 80 which led to higher surface free energy and uptake of water by the vesicle membrane with the result of increase in VS (ElMeshad and Mohsen, 2016). This observation matches that of Waleed

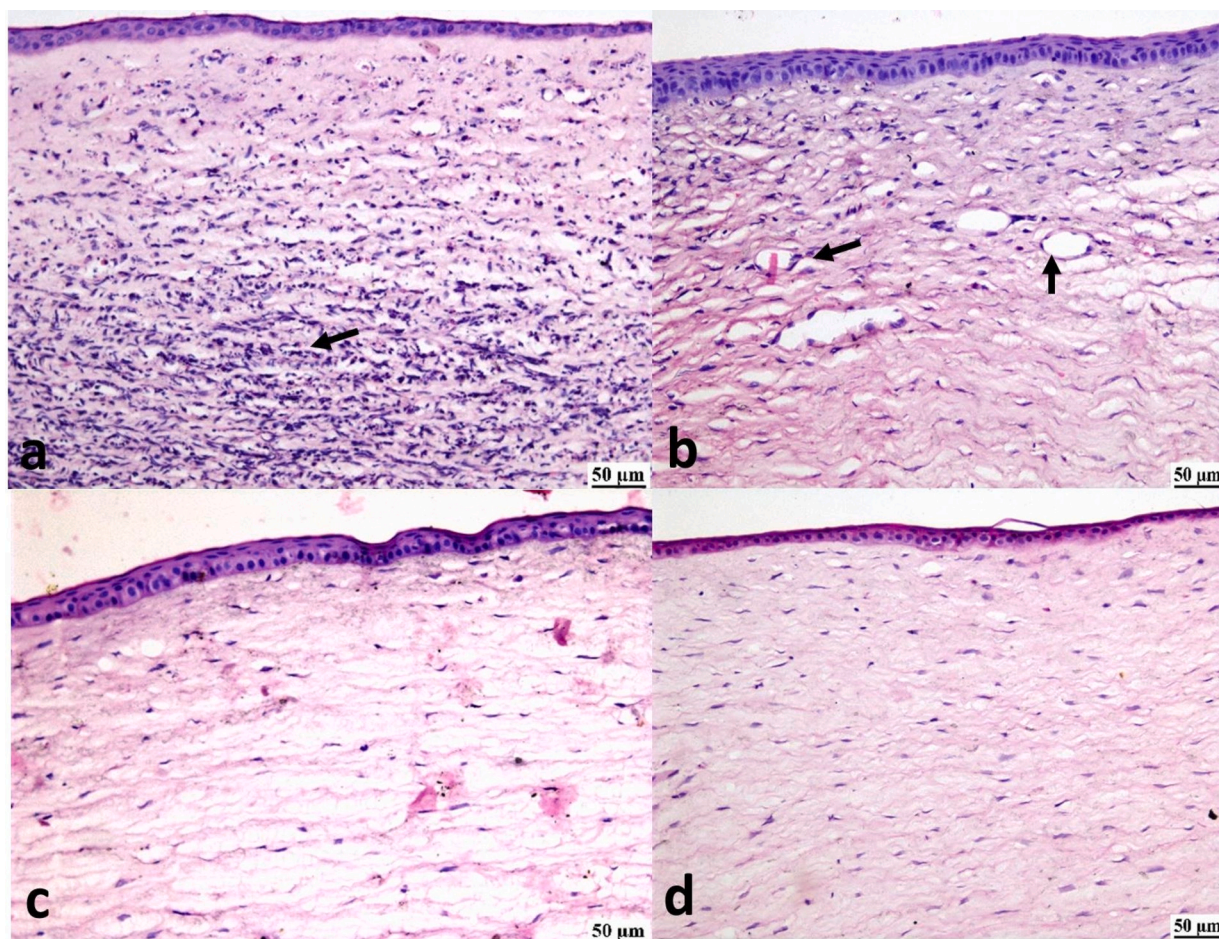


Fig. 11. Photomicrograph showing histopathologic evaluation (H&E) of the cornea in the different groups. (a) Showing marked inflammatory cells infiltration (arrow) in G-CO group. (b) Showing mild inflammatory edema (arrow) in G-OPT group. Apparently normal cornea in G-SPLs group (c) and in G-SPLs-SI group (d).

S. Alharbi et al. (Alharbi et al., 2022) who reported that increasing the HLB value of edge activator led to a significant increase in the size of flibanserine SPLs.

The PDI gives an indication of the size variation between particles and it ranges from 0 to 1 (Said et al., 2018). Table 2 shows that the PDI values of the prepared SPLs formulations range from  $0.124 \pm 0.28$  to  $0.562 \pm 0.07$ , indicating that they lied in the acceptable size range (Said et al., 2021).

ZP highlights the physical stability of the prepared formulations. Increasing the ZP value increases the repulsion between the vesicles with their subsequent decrease in aggregation and increases the stability of the system (Said et al., 2018). Formulations having zeta potential values less than  $-30$  or higher than  $+30$  are highly stable systems (Dave et al., 2017).

Table 2 shows that the ZP of the prepared SPLs formulations varied between  $-25.3 \pm 0.81$  and  $-38.6 \pm 0.20$  mV, indicating that most of SPLs formulations are physically stable (Zaki et al., 2022c). Effects of sonication time (X1), Span 60:

EA ratio (X2) and type of EA (X3) on ZP are shown in Fig. S3.

The linear model best fit the ZP data ( $p$  value  $<0.0001$ ) with an adequate precision of 10.1908 and a small difference between adjusted and predicted  $R^2$  (Table 1). The following equation shows the effect of the formulation variables on ZP:

$$ZP = -32.81 + 0.0271 \times 1 + 4.08X2a - 0.5330X2b + 0.1922 \times 3.$$

The zeta potential values are significantly affected by the Span60: EA ratio (X2) ( $p$ -values  $<0.0001$ ). The SPLs negative charge may be related to the partial negative groups present in the polar head of Span (Abdelrahman et al., 2017). The increase in Span60: EA ratio (X2) led to

a significant increase in the ZP absolute values which could be related to the increased concentration of negatively charged span 60 in the mixture compared to the nonionic EAs tween 80 and PVA. On the other hand, sonication time (X1) and type of EA (X3) have no significant effect on zeta potential values as shown in (Table S1).

### 3.2. Statistical analysis, optimization and validation

Using Design Expert® software, a numerical study was performed to find an optimal SPLs formulation, minimizing VS, ZP, and maximizing EE%. This resulted in an optimum SPLs formulation with a desirability of 0.919 which was selected for further analysis (Fig. 1). It had a Span60: Tween80 ratio of 6:1 with a sonication time of 9.5 mins. The predicted values for EE%, VS, and ZP were 85.355 %, 145.8 nm, and  $-36.5368$  mV respectively as given in Table 3. The optimum formula was prepared and validated as shown in Table 3, with a relative error of less than 5 % from the expected outcomes produced by the Design Expert software, confirming model fitness (Said et al., 2021; Said et al., 2017, 2018; Zaki et al., 2022a; Zaki et al., 2022c).

### 3.3. Evaluation of the optimum SPLs formula

#### 3.3.1. Transmission electron microscopy (TEM)

TEM imaging indicated reasonably spherical vesicles as shown in Fig. 2. There were no aggregates seen, which might be explained by the comparatively high ZP on the vesicle surfaces causing repulsion of the nearby SPLs (Dehghani et al., 2017).

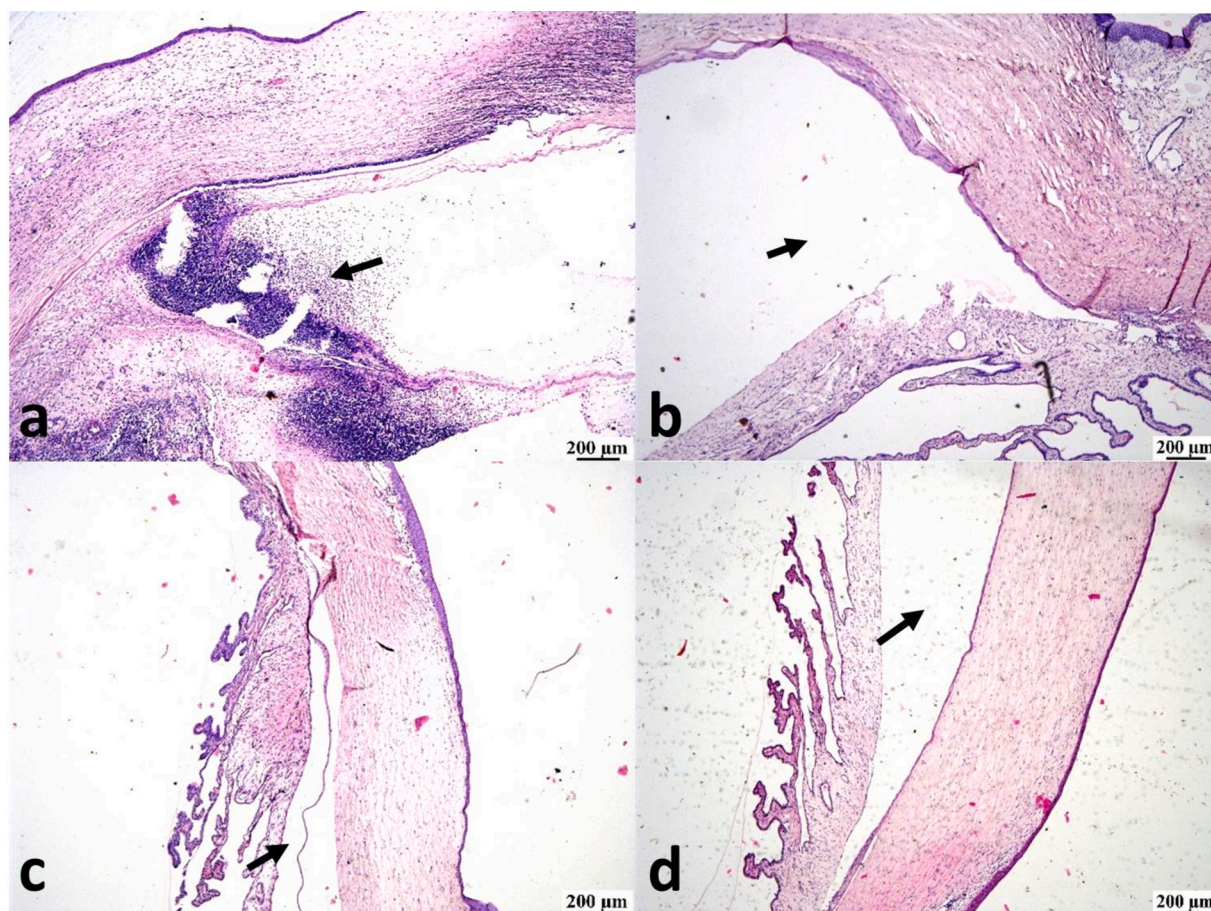


Fig. 12. Photomicrograph showing histopathologic evaluation (H&E) of the anterior chamber in the different groups. (a) Showing intense inflammatory cells infiltration (arrow) in G-CO group. Apparently normal anterior chamber (arrow) in G-OPT group (b), G-SPLs group (c) and in G-SPLs-SI group (d).

### 3.3.2. Study of the in-vitro release

Fig. 3 depicts a profile comparing the release of the optimized SPLs formulation to the PRED solution. When compared to the drug solution, the optimal SPLs formulation demonstrated a prolonged release profile of PRED. This could be due to the encapsulation of PRED inside the SPLs nanovesicles, in contrast to the drug suspension, which released 100 % of the drug during the first hour.

### 3.3.3. Study of the influence of aging

The stability of the optimized SPLs formulation after a month of storage is shown in Table 4. The EE%, VS, and ZP did not change significantly over the length of the experiment (7 and 30 days), showing that the optimum SPLs formula remained physically stable during storage at 4 °C (Zaki et al., 2022a; Zaki et al., 2022c).

## 3.4. Assessment of the optimum PRED loaded SPLs-SI

### 3.4.1. Visual appearance

The freeze-dried SPLs-SI was white with a sponge-like texture. It was hard enough to withstand handling but not so hard that they hurt the eye. The prepared SPLs-SI have a diameter of around 7 mm and a thickness of 1 mm.

### 3.4.2. Surface pH

The pH of all inserts ranged from 7 to 8, which corresponds to the physiological pH of the ocular surface. This reduces eye surface irritation, tears, and reflex blinking (Shukr, 2016).

### 3.4.3. Study of the mucoadhesion

Wetting was reported to play a function in bringing the mucoadhesive into touch with mucin, resulting in the formation of adhesive bonds 60, which resulted in the sustainment of ocular drug delivery (Wang and Bazos, 1983).

The SPLs-SI showed no displacement during the study period (1 h), indicating good mucoadhesive character.

### 3.4.4. Fourier-transform infrared (FTIR) spectroscopy

The FTIR spectrum of PRED (Fig. S4-A) showed characteristic peaks at 532.35, 705.95, 721.38, 802.39, 821.68, 860.25, 883.40, 987.55, 1037.70, 1099.43, 1242.16, 1300.02, 1365.60, 1411.89, 1442.75, 1608.63, 1658.78, 1716.65, 2935.56, 2987.95, 3008.95 and 3403.29  $\text{cm}^{-1}$ , some of which are decreased in intensity in the optimum SPLs formulation (Fig. S4-B) and the optimum PRED loaded SPLs-SI (Fig. S4-C) due to dilution effect while others disappeared indicating the entrapment of the drug in the optimum formulations (CHAUDHARI and DESAI, 2019; Hanafy et al., 2019).

### 3.4.5. Differential scanning calorimetry (DSC)

Water desorption due to heat is observed in PRED commencing at roughly 80 °C (Kocabas et al., 2023) (fig. S5-A). An endothermic peak was observed at 240 °C indicating the melting point of PRED (CHAUDHARI and DESAI, 2019). The DSC thermograms of optimum SPLs formula (fig. S5-B) and optimum PRED loaded SPLs-SI (fig. S5-C) showed the disappearance of the characteristic peak of PRED indicating the entrapment of PRED inside the SPLs and SPLs-SI in an amorphous state (Zaki et al., 2022a; Zaki et al., 2022c).

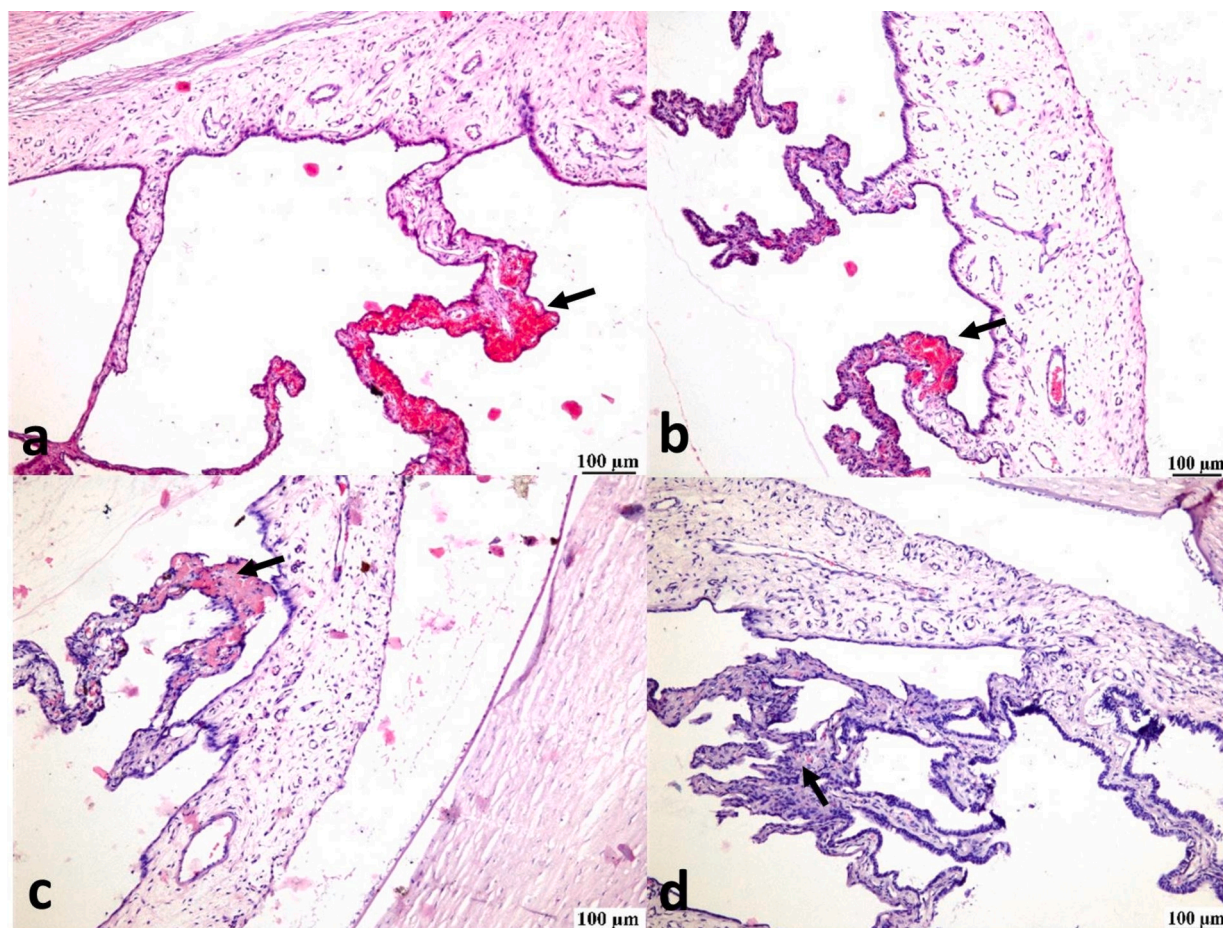


**Fig. 13.** Photomicrograph showing histopathologic evaluation (H&E) of the ciliary body in the different groups. (a) Showing diffuse hemorrhage (arrow) in G-CO group. Focal hemorrhage (arrow) in G-OPT group (b) and G-SPLs group (c). Mild inflammatory cells infiltration (arrow) in G-SPLs-SI group.

#### 3.4.6. Study of X-ray diffraction (XRD)

The XRD spectra of pure PRED, the optimized SPLs formulation and the optimized PRED loaded SPLs-SI are presented in Fig. S6. PRED spectrum showed characteristic sharp peaks indicating its crystallinity (Bouriche et al., 2021; Szegedi et al., 2020) (Fig. S6-A). While the XRD spectra of the optimized SPLs formulation and the optimized PRED loaded SPLs-SI showed a reduction in the intensity of some PRED peaks and the absence of others (Fig. S6-B and S6-C) (Zaki et al., 2022c) which could be related to the entrapment of PRED inside SPLs vesicles in an amorphous form which confirms the DSC results.

## 4. In-vivo studies

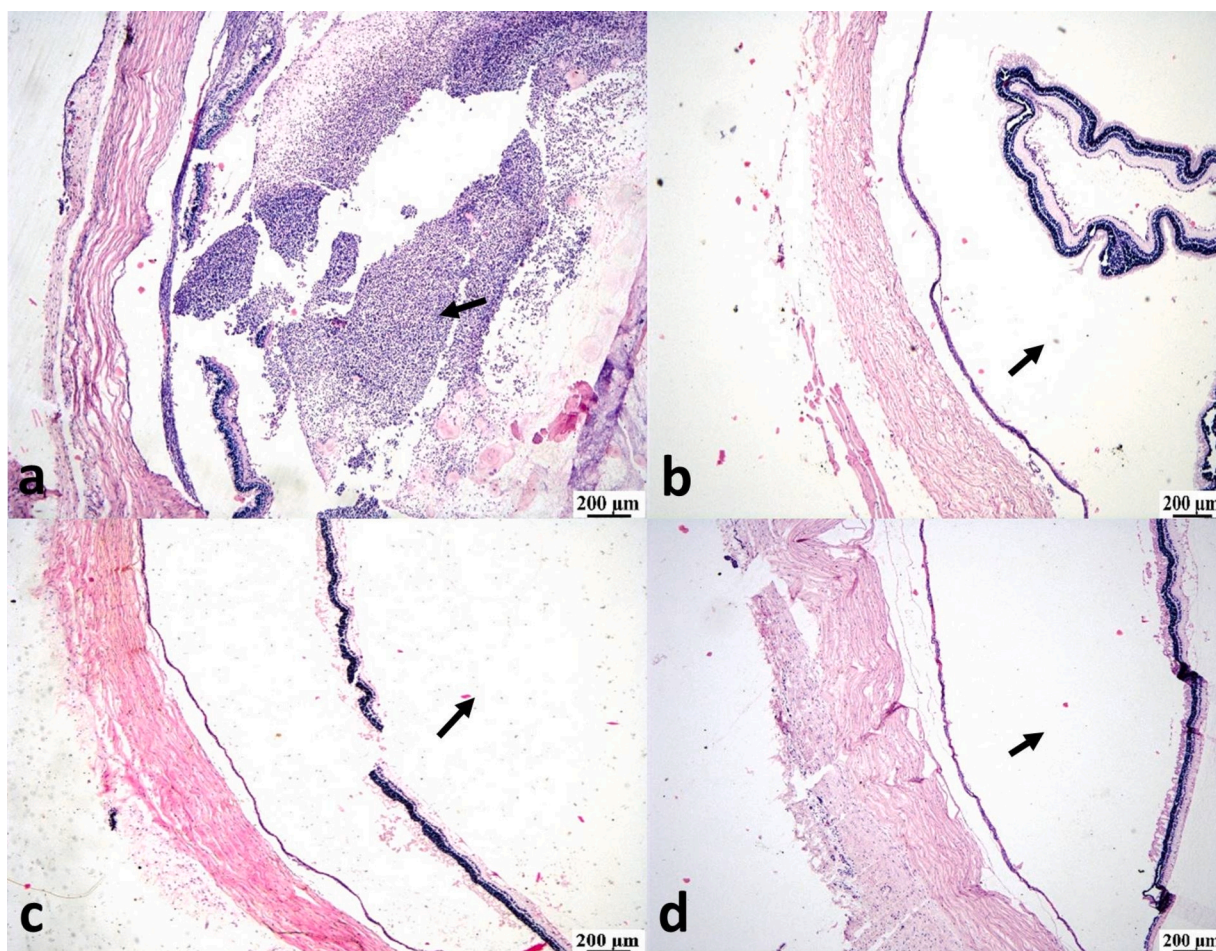
### 4.1. Ophthalmological findings and evaluation of uveitis in the treatment groups

Fig. 4 a and b showed induction of uveitis through intracameral injection of lipopolysaccharide (LPS) from *Escherichia coli*. The rabbits in this study showed significantly higher grades of ocular inflammation at 24 h after intracameral injection of endotoxin. Clinical signs of uveitis observed were: conjunctival hyperemia, congestion of episcleral and limbal blood vessels, hyphema, miosis, aqueous flare and iris neovascularization (Fig. 5a). Prednisolone loaded spanlastics spongy insert was applied successfully in the lower cul-de-sac of the G-SPLs-SI group (Fig. 5b). Higher grades of ocular inflammation were observed in the control group throughout the observation periods than the treatment groups. The score of the conjunctival hyperemia and congestion of episcleral and limbal blood vessels was high “4” in all treatment and

control groups for 5 days from the beginning of treatment. At 14 days, the group treated using prednisolone loaded spanlastics spongy insert (G-SPLs-SI) had a lowest score of  $0.33 \pm 0.47$  (range, 0–1), followed by the group treated with prednisolone loaded spanlastics (G-SPLs) that had a score of  $0.83 \pm 0.68$  (range, 0–2) and a high score was recorded in the control group (G-CO)  $3.33 \pm 0.47$  (range, 3–4). The group treated with commercially available prednisolone eye drops had a mean score of 2 by the end of week two from the beginning of treatment. These findings could be related to the elasticity of SPLs which enhances the corneal permeability of PRED (Abdelbari et al., 2021) in addition to the permeation enhancing effect of chitosan which transitory opens the tight connections between corneal cells promoting PRED passage through the corneal barrier (Janagam et al., 2017). Moreover, the positive charge of chitosan initiates an electrostatic interaction with the negative charge of the mucin coating the cornea, improving the mucoadhesive and corneal retention of PRED SPLs-SI over SPLs solution and commercial PRED solution which are rapidly drained from the eye surface (Wang et al., 2011). Also, chitosan has an anti-inflammatory effect (Chang et al., 2019) which synergizes the effect of PRED.

The corneal edema was recorded in all groups 48 h after induction and continued to decrease gradually in the treatment groups. The recorded mean scores by the end of week two were  $0.3 \pm 0.47$  (range, 0–1),  $0.83 \pm 0.68$  (range, 0–2),  $1.83 \pm 0.68$  (range, 1–3) and  $3.33 \pm 0.74$  (range, 2–4) in the G-SPLs-SI, G-SPLs, G-OPT and G-CO groups respectively, which could be related to the previously discussed reasons.

At the end of the study period, the G-SPLs-SI had a mean score of 0 for the following clinical signs of uveitis: hyphema, aqueous flare and iris neovascularization, and the G-SPLs had a mean score of  $0.16 \pm 0.37$



**Fig. 14.** Photomicrograph showing histopathologic evaluation (H&E) of the posterior chamber in the different groups. (a) Showing intense inflammatory cells infiltration (arrow) in G-CO group. Apparently normal posterior chamber (arrow) in G-OPT group (b), G-SPLs group (c) and in G-SPLs-SI group (d).

(range, 0–1) for the same clinical signs. Significantly higher scores were recorded in the G-CO and G-OPT groups respectively. The OPT-group had a mean score of  $0.33 \pm 0.47$  (range, 0–1) for the same clinical signs after 14 days treatment. The recorded scores for hyphema, aqueous flare and iris neovascularization in the control group were  $0.83 \pm 0.68$  (range, 0–2),  $2.33 \pm 0.47$  (range, 2–3) and  $3 \pm 0.57$  (range, 2–4) respectively.

Clinical signs and scores of uveitis observed at the evaluation periods in this study were shown in Table 5. Evaluation of the clinical signs of uveitis in the G-SPLs-SI group throughout the different observation periods were shown in Fig. 6. The clinical evaluation of G-SPLs, G-OPT and G-CO groups was presented in Fig. 7, Fig. 8 and Fig. 9 respectively.

All corneas were negative to fluorescein staining throughout the study. Slit-lamp examination revealed the complete loss of corneal transparency and the inability to evaluate the anterior segment of the eye in the G-CO group at the end of the study, and direct and indirect ophthalmoscopy were not possible in this group. Mild loss of corneal transparency was reported in G-OPT and G-SPLs groups. The mean intraocular pressure (IOP) measurement was within normal reference ( $20.3 \pm 3.02$  mmHg) range (15–25 mmHg). Regarding vision assessment, all eyes in the different groups retained the potential for vision by the end of the study.

#### 4.2. Histopathology

Microscopic examination of conjunctiva (Fig. 10) revealed intense diffuse mononuclear and neutrophilic cells infiltration, marked edema and thickened epithelial lining in G-CO group. G-OPT group showed

moderate inflammatory reaction in the conjunctiva while G-SPLs group exhibited mild edema and G-SPLs-SI group showed apparently normal conjunctiva.

Marked inflammatory cells infiltrations were detected in the corneas of G-CO group that resulted in thickened cornea and dispersion of corneal stroma. G-OPT group showed reduced inflammation severity with mild edema. Meanwhile, G-SPLs and G-SPLs-SI groups exhibited apparently normal corneas (Fig. 11). The anterior chamber of G-CO group was densely packed with intense inflammatory cells and fibrinous exudate. On the contrary, all treated groups showed apparently normal anterior chamber (Fig. 12). Diffuse hemorrhage was observed in the ciliary body of eye sections from G-CO group. G-OPT and G-SPLs groups showed focal hemorrhage in the ciliary body. G-SPLs-SI group exhibited mild inflammatory cells infiltration in this region (Fig. 13). Similar to the findings of the anterior chamber, the posterior chamber of G-CO group showed marked inflammation. However, apparently normal posterior chambers were observed in all treated groups (Fig. 14). G-CO group showed marked inflammatory cells infiltration in the choroid. G-OPT group showed mild inflammation while both G-SPLs and G-SPLs-SI groups exhibited apparently normal choroid (Fig. 15).

#### 4.3. Immunohistochemistry

##### 4.3.1. HSP90 expression

Intense HSP90 was detected in the uvea of eyes from G-CO group. Moderate HSP90 was observed in both G-OPT and G-SPLs groups (Fig. 16). The least positive expression was detected in the G-SPLs-SI group. Significant reduction in the expressed HSP90 was observed in all

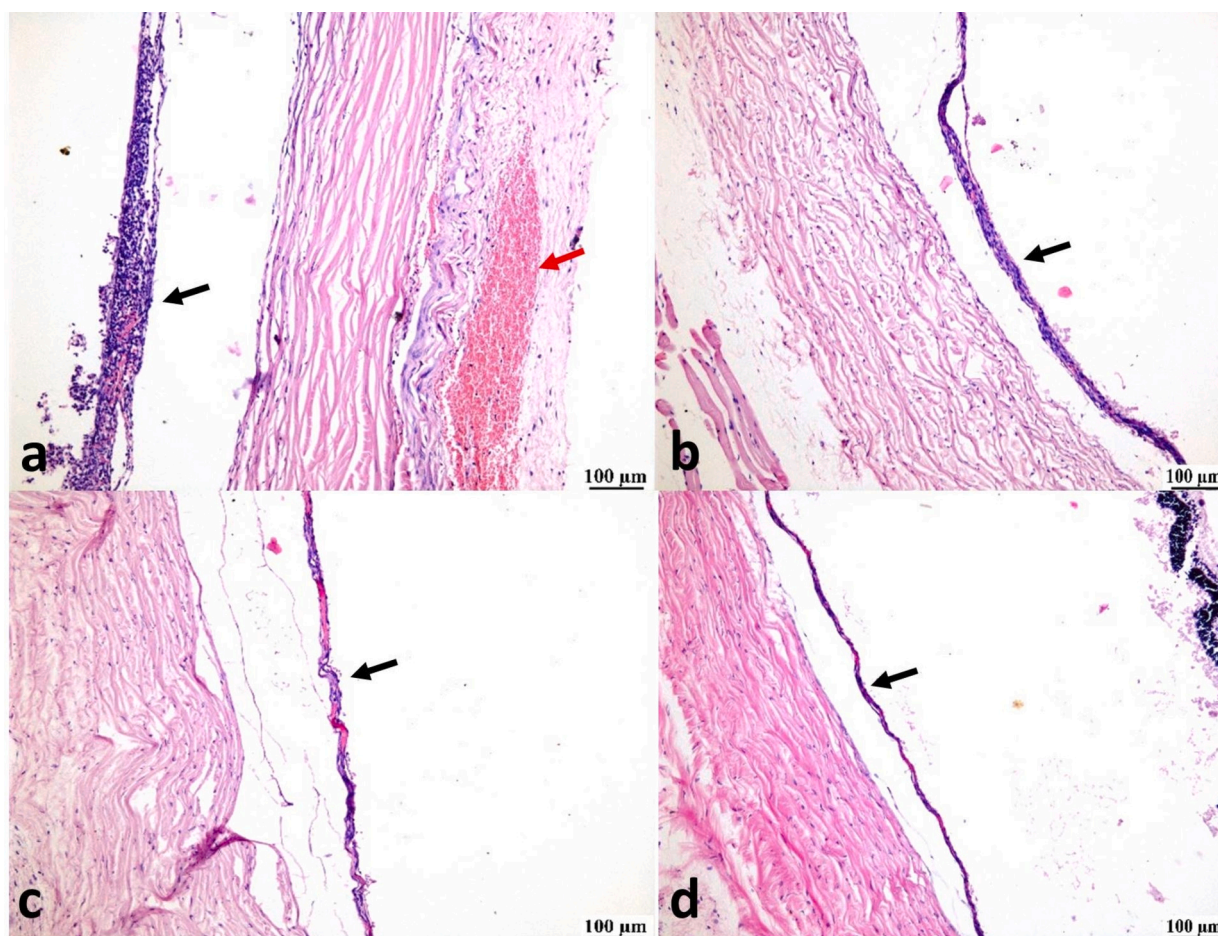


**Fig. 15.** Photomicrograph showing histopathologic evaluation (H&E) of the choroid in the different groups. (a) Showing intense inflammatory cells infiltration (black arrow) in G-CO group, note hemorrhage in sclera (red arrow). (b) Mild inflammatory cells infiltration (arrow) in G-OPT group. (c) Apparently normal choroid (arrow) in G-SPLs group and in G-SPLs-SI group (d). (For interpretation of the references to colour in this figure legend, the reader is referred to the web version of this article.)

treated groups in comparison to G-CO group. No significant difference was observed between G-OPT and G-SPLs groups (Fig. 17). These findings could be related to the previously discussed reasons under 4.1.

#### 4.4. Macroscopic examination of the gelling process, mucoadhesive behavior and biodegradation

The SPLs-SI absorbs fluid from the mucosa and forms a gel. This reduces the foreign body sensation associated with topical ocular administration of solid dose forms. It also has high mucoadhesive characteristics; it remained in contact with the eye for 12 h during the period of the study, and it completely disappeared after 24 h, indicating its biodegradation as shown in fig. S7.

#### 4.5. Ocular irritation test

The ocular Draize test showed no irritation signs after applying the SPLs-SI for the whole study period (24 h), as shown in fig. S7, the eye irritation reaction scores were 0, according to Draize's rating system. This indicated that the SPLs-SI is safe and biocompatible with the eye's surface, making it suitable for ocular drug delivery.

## 5. Conclusions

Spanlastics were simply prepared and then statistically optimized using an I-optimal design to achieve the composition with the maximum

ZP, EE%, and lowest VS. The optimum formula has a reasonable VS, surface charge, and PRED loading. When compared to the PRED solution, it demonstrated a sustained PRED release. Furthermore, it demonstrated good stability for one month. TEM pictures revealed spherical vesicles without aggregates. The optimum formulation was then loaded into chitosan sponge to further enhance its corneal permeation and ocular residence time through improving its mucoadhesive properties. FTIR, DSC, and XRD showed encapsulation of PRED inside the SPLs-SI. Then, the optimum SPLs-SI was involved in histopathological, immunohistochemistry and an in vivo study where it was capable of enhancing the anti-inflammatory effect of PRED with once daily application compared to commercial PRED solution which was given four times daily. It demonstrated quick gelation in the eye, minimizing foreign body sensation, as well as good mucoadhesion and biodegradability, requiring no removal from the eye. It has the potential to be a promising carrier for the ocular delivery of PRED.

#### CRediT authorship contribution statement

**Mayada Said:** Writing – original draft, Formal analysis, Data curation, Conceptualization. **Khaled M. Ali:** Writing – original draft, Visualization, Methodology, Data curation. **Munera M. Alfadhel:** Writing – review & editing, Resources, Investigation, Formal analysis. **Obaid Afzal:** Visualization, Validation, Formal analysis, Conceptualization. **Basmah Nasser Aldosari:** Validation, Project administration, Investigation, Funding acquisition. **Maha Alsunbul:** Visualization, Validation,

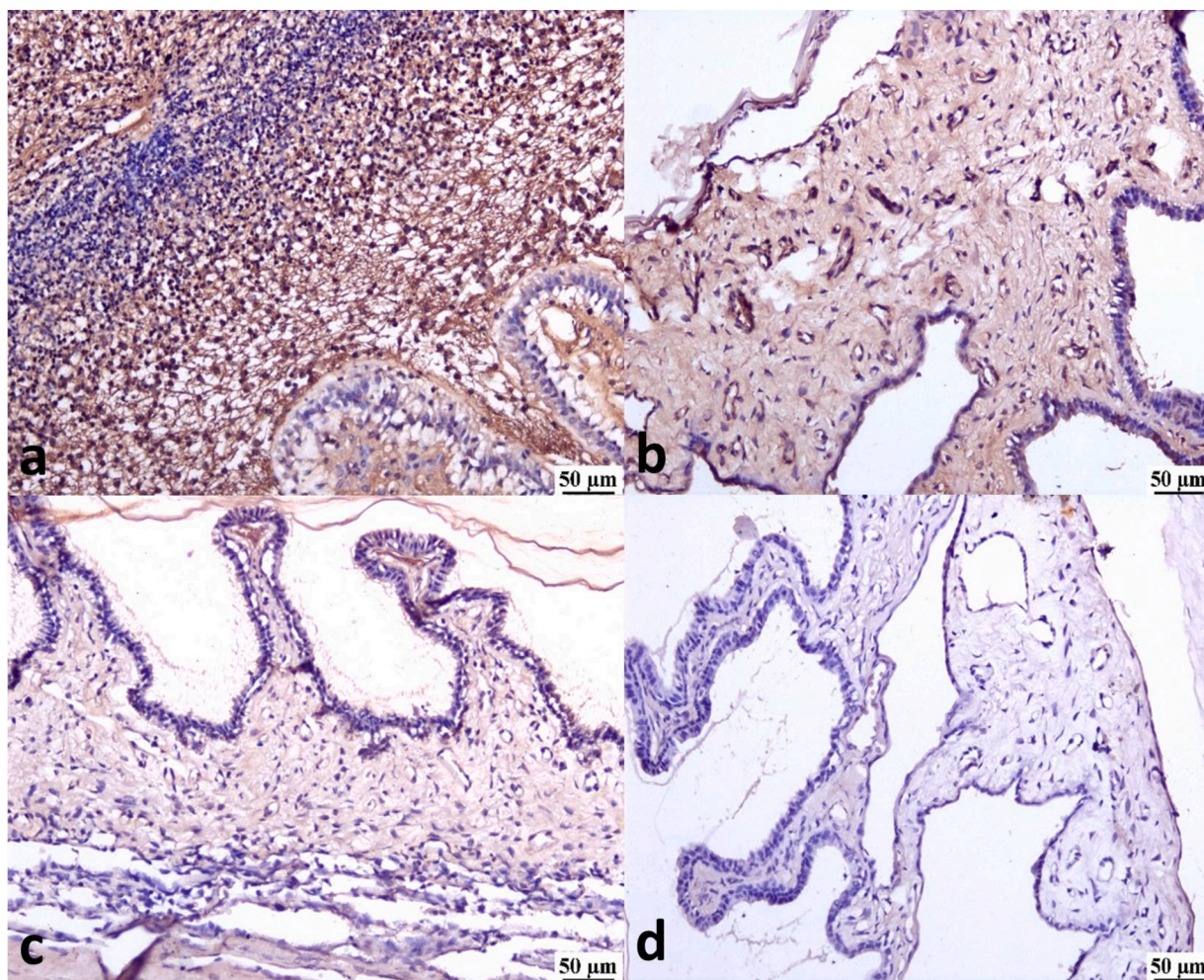


Fig. 16. Photomicrograph (Immune staining) showing HSP90 expression in the eyes of different groups; (a) intense HSP90 expression in G-CO group, moderate HSP90 expression in G-OPT group (b) and in G-SPLs group (c) and in mild HSP90 expression G-SPsNS group (d).

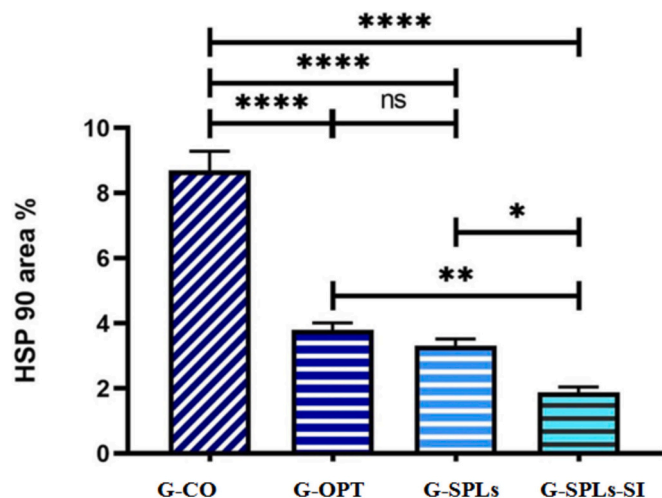


Fig. 17. Chart represents HSP90 expression. Data are presented as mean ± SE. Significant difference is considered at P<0.05.

Project administration, Funding acquisition. **Rawan Bafail:** Visualization, Resources, Project administration, Investigation. **Randa Mohammed Zaki:** Writing – review & editing, Software, Resources, Methodology.

#### Declaration of competing interest

The authors declare the following financial interests/personal relationships which may be considered as potential competing interests: Randa Mohammed Zaki reports financial support was provided by Prince Sattam bin Abdulaziz University. If there are other authors, they declare that they have no known competing financial interests or personal relationships that could have appeared to influence the work reported in this paper.

#### Acknowledgement

this study is supported via funding from Prince Sattam Bin Abdulaziz University Project number (PSAU/2024/R/1445). Also, the research was funded by Princess Nourah bint Abdulrahman University Researchers Supporting Project number (PNURSP2024R736), Princess Nourah bint Abdulrahman University, Riyadh, Saudi Arabia.

#### Appendix A. Supplementary data

Supplementary data to this article can be found online at <https://doi.org/10.1016/j.ijpx.2024.100293>.

#### Data availability

The data that has been used is confidential.

## References

- Abdelbari, M.A., El-Mancy, S.S., Elshafeey, A.H., Abdelbary, A.A., 2021. Implementing spanlastics for improving the ocular delivery of clotrimazole: in vitro characterization, ex vivo permeability, microbiological assessment and in vivo safety study. *Int. J. Nanomedicine* 6249–6261.
- Abdelrahman, F.E., Elsayed, I., Gad, M.K., Elshafeey, A.H., Mohamed, M.I., 2017. Response surface optimization, Ex vivo and in vivo investigation of nasal spanlastics for bioavailability enhancement and brain targeting of risperidone. *Int. J. Pharm.* 530, 1–11.
- Alharbi, W.S., Hareeri, R.H., Bazuhair, M., Alfaleh, M.A., Alhakamy, N.A., Fahmy, U.A., Alamoudi, A.A., Badr-Eldin, S.M., Ahmed, O.A., AlGhamdi, S.A., 2022. Spanlastics as a potential platform for enhancing the brain delivery of flibanserin: in vitro response-surface optimization and in vivo pharmacokinetics assessment. *Pharmaceutics* 14, 2627.
- Alonso, M.J., Sánchez, A., 2003. The potential of chitosan in ocular drug delivery. *J. Pharm. Pharmacol.* 55, 1451–1463.
- Badr-Eldin, S.M., Aldawsari, H.M., Alhakamy, N.A., Fahmy, U.A., Ahmed, O.A., Neamatallah, T., Tima, S., Almaghrabi, R.H., Alkudsi, F.M., Alamoudi, A.A., 2022. Merging experimental design and nanotechnology for the development of optimized simvastatin spanlastics: a promising combined strategy for augmenting the suppression of various human cancer cells. *Pharmaceutics* 14, 1024.
- Badria, F., Mazyed, E., 2020. Formulation of Nanospanlastics as a Promising Approach for improving the Topical delivery of a Natural Leukotriene Inhibitor (3-Acetyl-11-Keto- $\beta$ -Boswellic Acid): Statistical Optimization, in vitro Characterization, and ex vivo Permeation Study. *Drug Des. Devel. Ther.* 3697–3721.
- Bancroft, J.D., Gamble, M., 2008. *Theory and Practice of Histological Techniques*, 6th Edition. Churchill Livingstone, Elsevier, China.
- Bertram, U., Bodmeier, R., 2006. In situ gelling, bioadhesive nasal inserts for extended drug delivery: in vitro characterization of a new nasal dosage form. *Eur. J. Pharm. Sci.* 27, 62–71.
- Bouriche, S., Alonso-García, A., Cárceles-Rodríguez, C.M., Rezgui, F., Fernández-Varón, E., 2021. An in vivo pharmacokinetic study of metformin nanoparticles as an oral sustained release formulation in rabbits. *BMC Vet. Res.* 17, 1–11.
- Bucolo, C., Drago, F., Salomone, S., 2012. Ocular drug delivery: a clue from nanotechnology. *Front. Pharmacol.* 3, 188.
- Chang, S.-H., Lin, Y.-Y., Wu, G.-J., Huang, C.-H., Tsai, G.-J., 2019. Effect of chitosan molecular weight on anti-inflammatory activity in the RAW 264.7 macrophage model. *Int. J. Biol. Macromol.* 131, 167–175.
- Chaudhari, P.D., Desai, U.S., 2019. Formulation and evaluation of niosomal in situ gel of prednisolone sodium phosphate for ocular drug delivery. *International Journal of Applied Pharmaceutics* 97–116.
- Conrady, C.D., Yeh, S., 2021. A review of ocular drug delivery platforms and drugs for infectious and noninfectious uveitis: the past, present, and future. *Pharmaceutics* 13, 1224.
- Dave, V., Yadav, R.B., Kushwaha, K., Yadav, S., Sharma, S., Agrawal, U., 2017. Lipid-polymer hybrid nanoparticles: Development & statistical optimization of norfloxacin for topical drug delivery system. *Bioactive materials* 2, 269–280.
- Dehghani, F., Farhadian, N., Golmohammadzadeh, S., Birihae, A., Ebrahimi, M., Karimi, M., 2017. Preparation, characterization and in-vivo evaluation of microemulsions containing tamoxifen citrate anti-cancer drug. *Eur. J. Pharm. Sci.* 96, 479–489.
- El Zaafarany, G.M., Awad, G.A., Holayel, S.M., Mortada, N.D., 2010. Role of edge activators and surface charge in developing ultradeformable vesicles with enhanced skin delivery. *Int. J. Pharm.* 397, 164–172.
- El-Helw, A.-R.M., Fahmy, U.A., 2015. Improvement of fluvastatin bioavailability by loading on nanostructured lipid carriers. *Int. J. Nanomedicine* 5797–5804.
- ElMeshari, A.N., Mohsen, A.M., 2016. Enhanced corneal permeation and antimycotic activity of itraconazole against *Candida albicans* via a novel nanosystem vesicle. *Drug Deliv.* 23, 2115–2123.
- Elsaied, E.H., Dawaba, H.M., Ibrahim, E., Afouna, M.I., 2019. Effect of pegylated edge activator on Span 60 based nanovesicles: comparison between Myrj 52 and Myrj 59. *Universal Journal of Pharmaceutical Research* 4, 1–8.
- Foo, K.S., Bavoh, C.B., Lal, B., Mohd Shariff, A., 2020. Rheology impact of various hydrophilic-hydrophobic balance (HLB) index non-ionic surfactants on cyclopentane hydrates. *Molecules* 25, 3725.
- Gaafar, P.M., Abdallah, O.Y., Farid, R.M., Abdelkader, H., 2014. Preparation, characterization and evaluation of novel elastic nano-sized niosomes (ethoniosomes) for ocular delivery of prednisolone. *J. Liposome Res.* 24, 204–215.
- Gaudana, R., Ananthula, H.K., Parenky, A., Mitra, A.K., 2010. Ocular drug delivery. *AAPS J.* 12, 348–360.
- Ghaderi, S., Ghanbarzadeh, S., Mohammadhassani, Z., Hamishehkar, H., 2014. Formulation of gammaoryzanol-loaded nanoparticles for potential application in fortifying food products. *Advanced Pharmaceutical Bulletin* 4, 549.
- Grassiri, B., Zambito, Y., Bernkop-Schnürch, A., 2021. Strategies to prolong the residence time of drug delivery systems on ocular surface. *Adv. Colloid Interf. Sci.* 288, 102342.
- Greaves, J.L., Wilson, C.G., 1993. Treatment of diseases of the eye with mucoadhesive delivery systems. *Adv. Drug Deliv. Rev.* 11, 349–383.
- Han, T., Nwe, N., Furuike, T., Tokura, S., Tamura, H., 2012. Methods of N-Acetylated Chitosan Scaffolds and its in-Vitro Biodegradation by Lysozyme.
- Hanafy, A.F., Abdalla, A.M., Guda, T.K., Gabr, K.E., Royall, P.G., Alqurshy, A., 2019. Ocular anti-inflammatory activity of prednisolone acetate loaded chitosan-deoxycholate self-assembled nanoparticles. *Int. J. Nanomedicine* 3679–3689.
- Hosseinzadeh, H., Atyabi, F., Dinarvand, R., Ostad, S.N., 2012. Chitosan–Pluronic nanoparticles as oral delivery of anticancer gemcitabine: preparation and in vitro study. *Int. J. Nanomedicine* 1851–1863.
- Ibrahim, M.M., Abd-Elgawad, A.-E.H., Soliman, O.A.-E., Jablonski, M.M., 2016. Stability and ocular pharmacokinetics of celecoxib-loaded nanoparticles topical ophthalmic formulations. *J. Pharm. Sci.* 105, 3691–3701.
- Jabs, D., Nussenblatt, R., Rosenbaum, J., Group SoUNSW, 2005. Standardization of uveitis nomenclature for reporting clinical data. Results of the first International Workshop. *Am. J. Ophthalmol.* 140, 509516.
- Janagam, D.R., Wu, L., Lowe, T.L., 2017. Nanoparticles for drug delivery to the anterior segment of the eye. *Adv. Drug Deliv. Rev.* 122, 31–64.
- Kakkar, S., Kaur, I.P., 2011. Spanlastics—a novel nanovesicular carrier system for ocular delivery. *Int. J. Pharm.* 413, 202–210.
- Kantaria, T., Kantaria, T., Heiduschka, P., Eter, N., Tugushi, D., Katsarava, R., 2023. Dexamethasone-Loaded Pseudo-Protein Nanoparticles for Ocular Drug Delivery: Evaluation of Drug Encapsulation Efficiency and Drug Release, 2023. *Journal of Nanotechnology*.
- Karn, P.R., Kim, H.D., Kang, H., Sun, B.K., Jin, S.-E., Hwang, S.-J., 2014. Supercritical fluid-mediated liposomes containing cyclosporin a for the treatment of dry eye syndrome in a rabbit model: comparative study with the conventional cyclosporin a emulsion. *Int. J. Nanomedicine* 3791–3800.
- Katzer, T., Chaves, P., Bernardi, A., Pohlmann, A., Guterres, S.S., Ruver Beck, R.C., 2014. Prednisolone-loaded nanocapsules as ocular drug delivery system: development, in vitro drug release and eye toxicity. *J. Microencapsul.* 31, 519–528.
- Khafagy, E.-S., Abu Lila, A.S., Sallam, N.M., Sanad, R.A.-B., Ahmed, M.M., Ghorab, M.M., Alotaibi, H.F., Alalawi, A., Aldawsari, M.F., Alshahrani, S.M., 2022. Preparation and Characterization of a Novel Mucoadhesive Carvedilol Nanosponge: a Promising Platform for Buccal Anti-Hypertensive delivery. *Gels* 8, 235.
- Kim, S., 2018. Competitive biological activities of chitosan and its derivatives: antimicrobial, antioxidant, anticancer, and anti-inflammatory activities. *International journal of polymer science* 2018.
- Kocbas, L., Ayyoubi, S., Tajourishi, M., Quodbach, J., Vermonden, T., Kok, R., 2023. 3D-printed prednisolone phosphate suppositories with tunable dose and rapid release for the treatment of inflammatory bowel disease. *Int. J. Pharm.* 123639.
- Kuno, N., Fujii, S., 2011. Recent advances in ocular drug delivery systems. *Polymers* 3, 193–221.
- Le Bourlais, C., Acar, L., Zia, H., Sado, P.A., Needham, T., Leverage, R., 1998. Ophthalmic drug delivery systems—recent advances. *Prog. Retin. Eye Res.* 17, 33–58.
- Liu, S., Jones, L., Gu, F.X., 2012. Nanomaterials for ocular drug delivery. *Macromol. Biosci.* 12, 608–620.
- Liu, Y., Wang, Y., Yang, J., Zhang, H., Gan, L., 2019. Cationized hyaluronate acid coated spanlastics for cyclosporine a ocular delivery: Prolonged ocular retention, enhanced corneal permeation and improved tear production. *Int. J. Pharm.* 565, 133–142.
- Maggs, D.J., Miller, P.E., Ofri, R., 2017. *Slatter's Fundamentals of Veterinary Ophthalmology E-Book*. Elsevier Health Sciences.
- Mahmoud, D.B., Bakr, M.M., Al-Karmalawy, A.A., Moatasim, Y., El Taweel, A., Mostafa, A., 2022. Scrutinizing the feasibility of nonionic surfactants to form isotropic bicelles of curcumin: a potential antiviral candidate against COVID-19. *AAPS PharmSciTech* 23, 1–12.
- Mazyed, E.A., Abdelaziz, A.E., 2020. Fabrication of transgelosomes for enhancing the ocular delivery of acetazolamide: Statistical optimization, in vitro characterization, and in vivo study. *Pharmaceutics* 12, 465.
- Ngan, C.L., Basri, M., Lye, F.F., Fard Masoumi, H.R., Tripathy, M., Karjiban, R.A., Abdul-Malek, E., 2014. Comparison of process parameter optimization using different designs in nanoemulsion-based formulation for transdermal delivery of fullerene. *Int. J. Nanomedicine* 4375–4386.
- Refai, H., Tag, R., 2011. Development and characterization of sponge-like acyclovir ocular minitables. *Drug Deliv.* 18, 38–45.
- Rothova, A., Suttrop-van Schulten, M., Treffers, W.F., Kijlstra, A., 1996. Causes and frequency of blindness in patients with intraocular inflammatory disease. *Br. J. Ophthalmol.* 80, 332–336.
- Ruiz-Moreno, J., Thillaye, B., De Kozak, Y., 1992. Retino-choroidal changes in endotoxin-induced uveitis in the rat. *Ophthalmic Res.* 24, 162–168.
- Saher, O., Ghorab, D.M., Mursi, N.M., 2016. Levofloxacin hemihydrate ocular semi-sponges for topical treatment of bacterial conjunctivitis: Formulation and in-vitro/in-vivo characterization. *Journal of drug delivery science and technology* 31, 22–34.
- Sahoo, S.K., Dilnawaz, F., Krishnakumar, S., 2008. Nanotechnology in ocular drug delivery. *Drug Discov. Today* 13, 144–151.
- Said, M., Elsayed, I., Aboelwafa, A.A., Elshafeey, A.H., 2017. Transdermal agomelatine microemulsion gel: pyramidal screening, statistical optimization and in vivo bioavailability. *Drug Deliv.* 24, 1159–1169.
- Said, M., Elsayed, I., Aboelwafa, A.A., Elshafeey, A.H., 2018. A novel concept of overcoming the skin barrier using augmented liquid nanocrystals: Box-Behnken optimization, ex vivo and in vivo evaluation. *Colloids Surf. B: Biointerfaces* 170, 258–265.
- Said, M., Aboelwafa, A.A., Elshafeey, A.H., Elsayed, I., 2021. Central composite optimization of ocular mucoadhesive cubosomes for enhanced bioavailability and controlled delivery of voriconazole. *Journal of drug delivery science and technology* 61, 102075.
- Said, M., Elsayed, I., Aboelwafa, A.A., Elshafeey, A.H., Hassan, M., 2024. Ocular mucoadhesive and biodegradable sponge-like inserts for the sustained and controlled delivery of voriconazole; preparation, D-optimal factorial optimization and in-vivo evaluation. *J. Pharm. Sci.* 113 (4), 961–973.
- Salem, H.F., Kharshoum, R.M., Abou-Taleb, H.A., Farouk, H.O., Zaki, R.M., 2021. Fabrication and appraisal of simvastatin via tailored niosomal nanovesicles for

- transdermal delivery enhancement: in vitro and in vivo assessment. *Pharmaceutics* 13, 138.
- Seyfoddin, A., Shaw, J., Al-Kassas, R., 2010. Solid lipid nanoparticles for ocular drug delivery. *Drug Deliv.* 17, 467–489.
- Shukr, M.H., 2016. Novel in situ gelling ocular inserts for voriconazole-loaded niosomes: design, in vitro characterisation and in vivo evaluation of the ocular irritation and drug pharmacokinetics. *J. Microencapsul.* 33, 71–79.
- Shukr, M.H., Ismail, S., El-Hossary, G.G., El-Shazly, A.H., 2022. Spanlastics nanovesicular ocular insert as a novel ocular delivery of travoprost: Optimization using Box–Behnken design and in vivo evaluation. *J. Liposome Res.* 32, 354–364.
- Suttorp-Schulten, M., Rothova, A., 1996. The possible impact of uveitis in blindness: a literature survey. *Br. J. Ophthalmol.* 80, 844.
- Szegedi, A., Trendafilova, I., Mihaly, J., Lazar, K., Nemeth, P., Momekov, G., Momekova, D., Marinov, L., Nikolova, I., Popova, M., 2020. New insight on prednisolone polymorphs in mesoporous silica/maghemite nanocomposites. *Journal of drug delivery science and technology* 60, 102092.
- Teabagy, S., Wood, E., Bilsbury, E., Doherty, S., Janardhana, P., Lee, D.J., 2023. Ocular immunosuppressive microenvironment and novel drug delivery for control of uveitis. *Adv. Drug Deliv. Rev.* 114869.
- Thrimawithana, T.R., Young, S., Bunt, C.R., Green, C., Alany, R.G., 2011. Drug delivery to the posterior segment of the eye. *Drug Discov. Today* 16, 270–277.
- Wang, P., Bazos, M., 1983. *Polymer Surface Interactions in the Biological Environment. Physicochemical Aspects of Polymer surfaces.* Plenum Press, New York, pp. 143–198.
- Wang, J.J., Zeng, Z.W., Xiao, R.Z., Xie, T., Zhou, G.L., Zhan, X.R., Wang, S.L., 2011. Recent advances of chitosan nanoparticles as drug carriers. *Int. J. Nanomedicine* 6, 765.
- Weichbrod, R.H., Thompson, G.A., Norton, J.N., 2018. *Management of Animal Care and Use Programs in Research, Education, and Testing.* CRC Press Boca Raton.
- Zaki, R.M., Alfadhel, M.M., Alossaimi, M.A., Elsayaf, L.A., Devanathadesikan Seshadri, V., Almurshedi, A.S., Yusif, R.M., Said, M., 2022a. Central Composite Optimization of Glycerosomes for the Enhanced Oral Bioavailability and Brain delivery of Quetiapine Fumarate. *Pharmaceutics* 15, 940.
- Zaki, R.M., Alfadhel, M.M., Alshahrani, S.M., Alsaqr, A., Al-Kharashi, L.A., Anwer, M.K., 2022b. Formulation of chitosan-coated brigatinib nanospanlastics: optimization, characterization, stability assessment and in-vitro cytotoxicity activity against H-1975 cell lines. *Pharmaceutics* 15, 348.
- Zaki, R.M., Seshadri, V.D., Mutayran, A.S., Elsayaf, L.A., Hamad, A.M., Almurshedi, A.S., Yusif, R.M., Said, M., 2022c. Wound healing efficacy of rosuvastatin transethosomal gel, I optimal optimization, histological and in vivo evaluation. *Pharmaceutics* 14, 2521.